

# The infrared side of galaxy formation.

## I. The local universe in the semi-analytical framework.

G.L. Granato<sup>1,4,5</sup>, C.G. Lacey<sup>2,3,4</sup>, L. Silva<sup>4,1</sup>, A. Bressan<sup>1</sup>, C.M. Baugh<sup>3</sup>, S. Cole<sup>3</sup>,  
C.S. Frenk<sup>3</sup>

### ABSTRACT

We present a new evolutionary model for predicting the far-UV to sub-mm properties of the galaxy population. This combines a semi-analytic galaxy formation model based on hierarchical clustering (GALFORM, Cole et al. 2000) with a spectro-photometric code which includes dust reprocessing (GRASIL, Silva et al. 1998). The former provides the star formation and metal enrichment histories, together with the gas mass and various geometrical parameters, for a representative sample of galaxies formed in different density environments. These quantities, together with a few other assumptions concerning the spatial distribution of dust and its optical properties, allow us to model the spectral energy distributions (SEDs) of galaxies, taking into account stellar emission and also dust extinction (absorption plus scattering) and re-emission. In the spectro-photometric code dust is considered only in the disk, but the general radiation field is contributed by both the disk and the bulge components with their own distinct age and metallicity distributions. Two phases are considered for the dust: molecular cloud complexes, where stars are assumed to be born, and the diffuse interstellar medium. The model includes both galaxies forming stars quiescently in disks, and starbursts triggered by galaxy mergers. We test our models against the observed spectro-photometric properties of galaxies in the local Universe, assuming a CDM cosmology with  $\Omega_0 = 0.3$  and  $\Lambda_0 = 0.7$ . The models reproduce fairly well the SEDs of normal spirals and starbursts from the far-UV to the sub-mm, and their internal extinction properties. The starbursts follow the observed relationship between the FIR to UV luminosity ratio and the slope of the UV continuum. They also reproduce the observed starburst attenuation law (Calzetti et al. 1999). This result is remarkable, because we use a dust mixture which reproduces the Milky Way extinction law. It suggests that the observed attenuation law is closely related to the geometry of the stars and dust. We compute galaxy luminosity functions over a wide range of wavelengths, which turn out to be in good agreement with observational data in the UV (2000Å), in the B and K bands, and in the IR (12 – 100 $\mu$ m). Finally, we investigate the reliability of some star formation indicators which are based on the properties of the continuum SEDs of galaxies. The UV continuum turns out to be a poor star formation indicator for our models, whilst the infrared luminosity is much more reliable.

*Subject headings:* Galaxies: evolution; Galaxies: formation; Galaxies: fundamental parameters; Galaxies: interactions; Galaxies: starburst; Infrared: galaxies; Ultraviolet: galaxies

---

<sup>1</sup>Osservatorio Astronomico di Padova, Vicolo dell'Osservatorio, 5, I-35122 Padova, Italy

<sup>2</sup>Theoretical Astrophysics Center, Juliane Maries Vej 30, 2100 Copenhagen Ø, Denmark

<sup>3</sup>Physics Department, Durham University, South Road, Durham DH1 3LE, UK

<sup>4</sup>SISSA, Via Beirut 2-4, I-34014 Trieste, Italy

<sup>5</sup>granato@pd.astro.it

### 1. Introduction

In recent years, our understanding of galaxy formation and evolution has advanced very rapidly, as a result of both observations and theory. On the observational side, new instruments have allowed the direct study of galaxy populations at

different wavelengths out to  $z \lesssim 5$ . By combining observations in the UV, optical, IR and sub-mm, we can now start to reconstruct the history of star formation in galaxies over the epochs when the bulk of the stars have formed (e.g. Madau et al. 1996; Steidel et al. 1999; Hughes et al. 1998). On the theoretical side, models based on the paradigm of structure formation through hierarchical clustering (which has successfully confronted a wide range of observations on large scale structure and microwave background anisotropies) have now been developed to the point where they can make definite predictions for the observable properties of galaxies (luminosities, colours, sizes, morphologies etc) at all redshifts, starting from an assumed initial spectrum of density fluctuations. The key technique for making these predictions has been that of *semi-analytical modelling* (White & Frenk 1991; Lacey & Silk 1991; Kauffmann et al. 1993; Cole et al. 1994; Somerville & Primack 1999). In this technique, one applies simplified analytical descriptions of the main physical processes of gas cooling and collapse, star formation, feedback effects from supernovae, galaxy merging etc, with the backbone being a Monte Carlo description of the process of formation and merging of dark matter halos through hierarchical clustering. The predicted star formation histories are then combined with detailed stellar population models to calculate galaxy luminosities at different wavelengths. Conversely, direct numerical simulations have been enormously successful in studying the evolution of structure in the dark matter on a huge range of scales (e.g. Jenkins et al. 1998), but currently do not have sufficient spatial resolution to simultaneously follow all the processes involved in galaxy formation.

The semi-analytical models have been successful in predicting and/or explaining a large range of galaxy properties, both at low and high redshift, for instance, luminosity functions and colours in different optical and near-IR bands (Lacey et al. 1993; Kauffmann et al. 1993; Cole et al. 1994), the mixture of galaxy morphologies and the evolution of elliptical galaxies (Kauffmann et al. 1993; Baugh et al. 1996; Kauffmann 1996), the properties of Lyman-break galaxies at high redshift (Baugh et al. 1998; Governato et al. 1998), the sizes and circular velocities of galaxies (Cole et al. 2000), and galaxy clustering evolution and the na-

ture of the clustering bias (Kauffmann et al. 1997; Baugh et al. 1999; Diaferio et al. 1999; Benson et al. 2000). However, with very few exceptions, these semi-analytical models have ignored both extinction and emission by interstellar dust, and calculated only the direct stellar emission in the UV, optical and near-IR. This has been partly because the importance of dust was generally underappreciated, especially for high redshift galaxies, but also because of the lack of physically realistic models for predicting dust effects.

This situation has now begun to change. On the one hand, there have been several observational discoveries demonstrating the importance of dust effects for building a complete picture of galaxy formation. (1) The discovery of a cosmic far-IR/sub-mm background by the COBE satellite (Puget et al. 1996; Guiderdoni, et al. 1997; Dwek, et al. 1998; Fixsen et al. 1998; Hauser et al. 1998; Schlegel et al. 1998), whose energy density indicates that, as suggested already by Wang (1991) and Franceschini et al. (1994), a large fraction of the energy radiated by stars over the history of the universe has been reprocessed by dust. (2) The discovery that the population of star forming galaxies at  $z \sim 2 - 4$  that have been detected through their strong Lyman-break features are substantially extinguished in the rest-frame UV (Pettini et al. 1998; Steidel et al. 1999). (3) The discovery of a population of sub-mm sources at high redshift ( $z \gtrsim 1$ ) using SCUBA, whose luminosities, if they are powered by star formation in dust-enshrouded galaxies, imply very large star formation rates ( $\sim 10^2 M_{\odot} \text{yr}^{-1}$ ), and a total star formation density comparable to what is inferred from the UV luminosities of the Lyman-break galaxies (Smail et al. 1997; Hughes et al. 1998; Lilly et al. 1999). (4) The ISO detection of a population of strong IR sources; 15  $\mu\text{m}$  ISOCAM (e.g. Oliver, et al. 1997; Elbaz, et al. 1999) and 175  $\mu\text{m}$  ISOPHOT surveys (e.g. Kawara, et al. 1998; Puget, et al. 1999) indicate a population of actively star forming galaxies at  $0.4 \lesssim z \lesssim 1.3$ , which boosts the cosmic star formation density by a factor  $\sim 3$  with respect to that estimated in the optical from the CFRS (Flores et al. 1999). For (1) and (3), there is the caveat that the contribution from dust-enshrouded AGNs to the sub-mm counts and background is currently uncertain, but probably the AGNs do not dominate (Granato et

al. 1997; Almaini et al. 1999; Madau 1999). These discoveries demonstrate that in order to understand the history of star formation in the universe from observational data, one must have a unified picture that covers all wavelengths from the far-UV to the sub-mm. The UV and the far-IR are especially important, since young stellar populations emit most of their radiation in the rest-frame UV, but a significant fraction of this is dust reprocessed into the rest-frame far-IR.

On the theoretical side, it is now possible for the first time to construct true *ab initio* models in which the galaxy formation itself and stellar emission and dust absorption and emission are calculated from first principles, based on physical models, and avoiding observational parameterizations for various key ingredients (e.g. shape of the luminosity function, dependence of dust temperature on galaxy properties). These new models, which provide a unified treatment of emission from stars and dust, and predict the evolution of galaxy luminosities from the far-UV to the mm, are the subject of this paper.

The effects of dust on galaxy luminosities at different wavelengths have been included in some previous galaxy evolution models, at various levels of sophistication, but mostly in the context of *backwards evolution* models, where one tries to evolve back from observed galaxy properties at the present day, in contrast to the *semi-analytical* models, where one evolves forward from cosmological initial conditions. In backwards evolution models, one starts from the observed luminosity functions of different types of galaxy at the present day, assumes a different star formation history for each type, and calculates the luminosity evolution for each type, to predict what the galaxy population would have looked like in the past. Guiderdoni & Rocca-Volmerange (1987) were the first to include *dust absorption* in a model of this type, based on a 1D slab model for the star and dust distribution, and calculating the dust content self-consistently from a chemical evolution model. The same treatment of dust was later used in the semi-analytical galaxy formation models of Lacey et al. (1993). In both cases, the models were used to calculate galaxy luminosities and number counts in the UV and optical. Mazzei et al. (1992) were the first to try to model the evolution of stellar emission and dust emission together in a consistent

framework based on stellar population synthesis models and a physical calculation of dust absorption. This model was then used by Franceschini et al. (1994) to calculate galaxy evolution and number counts in bands from the optical through to the far-IR, based on the backwards evolution approach. However, these models still made a number of simplifying assumptions (e.g. slab geometry for disks), and set a number of present-day properties of galaxies from observations (e.g. the optical depth of galactic disks, and the intensity of the radiation field heating the dust), rather than predicting them. Simpler backwards evolution models, where the luminosity evolution is parameterized as a simple function of redshift, have been considered by, e.g. Pearson & Rowan-Robinson (1996).

Recently, dust absorption has been included in several different semi-analytical models (Kauffmann et al. 1999; Somerville & Primack 1999; Cole et al. 2000). The first two calculate dust effects only for present-day galaxies, using a 1D slab model, and taking the dust optical depth from observational measurements. On the other hand, Cole et al. (2000) predict the dust optical depth and how it evolves, based on chemical evolution and a prediction of disk sizes, and use the 3D disk+bulge radiative transfer models of Ferrara et al. (1999) to calculate the dust attenuation. The only previous semi-analytical model to calculate dust emission as well as absorption is that of Guiderdoni et al. (1998). However, that model also has several limitations: the galaxy formation model does not include merging of either dark halos or visible galaxies, and the fraction of star formation occurring in bursts is simply an arbitrary function; dust absorption is again modelled assuming a 1D slab geometry; and the dust temperature distribution is not predicted. Instead, the dust emission spectrum is modelled as the sum of several components, whose temperatures and relative strengths are chosen so as to reproduce the observed correlations of IR colours with IR luminosity found by IRAS.

The present paper represents a major advance over this earlier work in terms of scope, physical self-consistency and predictiveness. We combine the semi-analytical galaxy formation model of Cole et al. (2000) with the stellar population + dust model of Silva et al. (1998). The galaxy

formation model includes formation of dark halos through merging, cooling and collapse of gas in halos to form disks, star formation in disks regulated by energy input from supernovae, merging of disk galaxies to form elliptical galaxies and bulges, bursts of star formation triggered by these mergers, predictions of the radii of disks and spheroids, and chemical enrichment of the stars and gas. The stellar population + dust model includes a realistic 3D geometry, with a disk and bulge, two phase dust in clouds and in the diffuse ISM, star formation in the clouds, radiative transfer of starlight through the dust distribution, a realistic dust grain model including PAHs and quantum heating of small grains, and a direct prediction of the dust temperature distribution at each point in the galaxy based on a calculation of dust heating and cooling. The output is the luminosity and spectrum of the stellar populations attenuated by dust, and of the dust emission from grains at a range of temperatures. From this, we can calculate the distribution of galaxy properties at any redshift, including the complete spectrum of each galaxy in the model from the far-UV to the sub-mm.

In this paper we compare the predicted properties for local galaxies with a wide range of observational data. A future paper will be devoted to high- $z$  galaxies (Lacey et al. 2000). In Sections 2 and 3 we describe, respectively, the galaxy formation model and the spectrophotometric model. Section 4 describes how we generate model galaxy catalogues for both normal and starburst galaxies. The comparison with observations (SEDs, extinction properties, colors, etc.) is presented in Section 5 for spiral galaxies, and in Section 6 for starbursts. The model luminosity functions at different wavelengths are compared with observations in Section 7. Section 8 uses the models to predict the relationship between the star formation rate and the luminosities in various UV and IR bands, and to assess the accuracies of these as star formation indicators. Section 9 presents a summary and conclusions.

## 2. Semi-analytical galaxy formation model

We calculate the formation histories and global properties of galaxies using the semi-analytical galaxy formation model (GALFORM) of Cole et al. (2000), a development of that described in Cole

Table 1: Adopted values for GALFORM parameters.

<i>Cosmology</i>	
$\Omega_0$	0.3
$\Lambda_0$	0.7
$h$	0.7
$\Omega_b$	0.02
$\Gamma$	0.19
$\sigma_8$	0.93
<i>Star formation and feedback</i>	
$\epsilon_{\star\text{disk}}$	$6.7 \times 10^{-3}$
$\alpha_{\star}$	-1.5
$\alpha_{\text{hot}}$	2.0
$V_{\text{hot}}$ (km/s)	150.0
<i>Stellar populations</i>	
IMF	Kennicutt (1983)
$\Upsilon$	1.4
$p$	0.02
$R$	0.29
<i>Mergers and bursts</i>	
$f_{\text{ellip}}$	0.3
$\epsilon_{\star\text{burst}}$	0.5
$\eta$	0.1

et al. (1994) and Baugh et al. (1998). The principle of the model is to calculate the formation and evolution of dark matter halos starting from an assumed cosmology and initial spectrum of density fluctuations, and then to calculate the evolution of the baryons (gas and stars) within these evolving halos using a set of simple, physically-motivated rules to model gas cooling, star formation, supernova feedback and galaxy mergers. We describe here only the main features of the model, and refer the reader to Cole et al. (2000) for more details and for a discussion of the effects of varying parameters with respect to standard values given in Table 1.

**(a) Cosmology:** The cosmology is specified by the present-day density parameter  $\Omega_0$ , cosmological constant  $\Lambda_0$ , baryon fraction  $\Omega_b$  (all in units of the critical density) and the Hubble constant  $H_0 = 100h \text{ km s}^{-1}\text{Mpc}^{-1}$ . We assume a cold dark matter (CDM) model, with the initial spectrum of density fluctuations having shape parameter  $\Gamma$  and amplitude  $\sigma_8$  (the r.m.s. density fluctuation in a sphere of radius  $8h^{-1}\text{Mpc}$ ).

**(b) Halo evolution:** Dark matter halos form through a process of hierarchical clustering, building up through merging from smaller objects. At any cosmic epoch, we calculate the number density of halos as a function of mass from the Press-Schechter (1974) formula. We then calculate halo merger histories, describing how a halo has formed, for a set of halos of different masses, using a Monte-Carlo algorithm based on the extended Press-Schechter formalism. We generate many different realizations of the merger history for each halo mass. We then follow the process of galaxy formation separately for each of these realizations.

**(c) Cooling and collapse of gas in halos:** Diffuse gas is assumed to be shock-heated to the virial temperature of the halo when it collapses, and to then cool radiatively out to a radius determined by the density profile of the gas and the halo lifetime. The gas which cools collapses to form a rotationally supported disk, for which the half-mass radius  $r_{\text{disk}}$  is calculated assuming that dark matter and associated gas are spun up by tidal torques, and that the angular momentum of the gas is conserved during the collapse. The gas supply by cooling is assumed to be continuous over the lifetime of the halo.

**(d) Star formation in disks:** Stars form from the cold gas in the disk, at a rate

$$\psi = M_{\text{cold}}/\tau_{\star\text{disk}}, \quad (1)$$

where the star formation timescale is assumed to be

$$\tau_{\star\text{disk}} = \epsilon_{\star\text{disk}}^{-1} \tau_{\text{disk}} (V_{\text{disk}}/200\text{km s}^{-1})^{\alpha_{\star}} \quad (2)$$

where  $V_{\text{disk}}$  is the circular velocity at the half-mass radius of the disk, and  $\tau_{\text{disk}} = r_{\text{disk}}/V_{\text{disk}}$  is the dynamical time.  $\epsilon_{\star\text{disk}}$  is the fraction of gas converted into stars in one dynamical time, for a galaxy with circular velocity  $V_{\text{disk}} = 200\text{km s}^{-1}$ . The scaling of the star formation timescale with dynamical time is motivated by observations of star formation in nearby galaxies (Kennicutt 1998), but modified to reproduce the observed dependence of gas fraction on luminosity.

**(e) Supernova feedback in disks:** The energy input from supernovae is assumed to reheat gas in the disk and eject it into the halo at a rate

$$\dot{M}_{\text{eject}} = \beta_{\text{disk}} \psi, \quad (3)$$

where for  $\beta_{\text{disk}}$  we assume

$$\beta_{\text{disk}} = (V_{\text{disk}}/V_{\text{hot}})^{-\alpha_{\text{hot}}} \quad (4)$$

Gas which has been ejected is assumed to be unavailable for cooling until the halo has doubled in mass through merging. The motivation for this parameterization is that the rate of gas ejection should be proportional to the rate of supernovae, and also depend on the escape velocity from the disk, which in turn is related to the circular velocity. Our standard case  $\alpha_{\text{hot}} = 2$  is equivalent to the assumption that a constant fraction of the Type II supernova energy goes into ejecting gas from the disk, if the escape velocity is proportional to  $V_{\text{disk}}$ .

**(f) Galaxy mergers and morphology:** The galaxy morphology (i.e. whether it is a spiral or elliptical) is determined by merging. Following the merger of two halos, the largest pre-existing galaxy is assumed to become the central galaxy in the new halo, while the other galaxies become satellite galaxies. The central galaxy can continue to grow a disk by cooling of gas from the halo. The satellite galaxies merge with the central galaxy on a timescale equal to that for dynamical friction to make the orbits decay. The merger is classed as a *major merger* if the mass ratio of the satellite to central galaxy exceeds a value  $f_{\text{ellip}}$ , and as a *minor merger* otherwise. In a *major merger*, any pre-existing stellar disks are destroyed, producing a stellar spheroid (elliptical galaxy or bulge), and any remaining cold gas is consumed in a burst of star formation. The star formation timescale in the burst is related to the dynamical time of the bulge as described below. The spheroid can grow a new disk by cooling of halo gas. In a *minor merger*, the stars from the satellite galaxy add to the bulge of the central galaxy, while the cold gas adds to the disk, but no burst is triggered. In either case, the half-mass radius  $r_{\text{bulge}}$  of the spheroid produced in a merger is calculated using an energy conservation argument. Galaxies are classified into different morphological types based on their bulge-to-disk luminosity ratios.

**(g) Star formation and feedback during bursts:** As already mentioned, star formation bursts are assumed to be triggered by major mergers of galaxies. In Cole et al. (2000), these bursts were modelled in a very simple way, with the conversion of gas into stars being assumed to be instantaneous, since the galaxy properties examined there were not sensitive to the detailed time dependence. In this paper, we model the bursts in more detail. We assume that star formation during bursts follows a law analogous to that for star formation in disks:

$$\psi = M_{\text{cold}}/\tau_{\star\text{burst}}, \quad (5)$$

with star formation timescale

$$\tau_{\star\text{burst}} = \epsilon_{\star\text{burst}}^{-1} \tau_{\text{bulge}} \quad (6)$$

where  $\tau_{\text{bulge}} = r_{\text{bulge}}/V_{\text{bulge}}$  is the dynamical time of the spheroid formed in the merger,  $V_{\text{bulge}}$  being the circular velocity at  $r_{\text{bulge}}$ . As in Cole et al. (2000), feedback is modelled as in disks except with  $V_{\text{bulge}}$  replacing  $V_{\text{disk}}$  in eqn.(4), assuming the same values for  $V_{\text{hot}}$  and  $\alpha_{\text{hot}}$ , giving a feedback factor  $\beta_{\text{burst}}$ . Since we assume that no new gas is supplied by cooling during the burst, the star formation rate and cold gas mass decay during the burst as  $\exp(-t/\tau_e)$ , where

$$\tau_e = \tau_{\star\text{burst}}/(1 - R + \beta_{\text{burst}}), \quad (7)$$

and  $R$  is the recycled fraction, discussed below. The burst is assumed to occur in a region of half-mass radius  $r_{\text{burst}}$ , where

$$r_{\text{burst}} = \eta r_{\text{bulge}} \quad (8)$$

More details on the geometry assumed for starbursts are given in § 3. For simplicity, the metallicity of the gas in the burst and of the stars formed during the burst are taken to be constant, and equal to the mean metallicity of the stars formed during the burst as calculated by the GALFORM model. The star formation in a burst is truncated at a time  $5\tau_e$  after the burst began, i.e. after 99% of the gas in the burst has either been converted into stars or blown out of the galaxy by supernova feedback. At this time, the remaining gas and dust in the burst region are assumed to be dispersed. Star formation then starts again in a normal galactic disk surrounding the bulge, if one has formed by cooling of halo gas since the major merger that triggered the burst.

**(h) Chemical evolution:** We assume that a fraction  $1/\Upsilon$  of the mass formed into stars goes into visible stars ( $0.1 < m < 125M_{\odot}$ ), while the remainder goes into brown dwarfs ( $m < 0.1M_{\odot}$ ). For visible stars we adopt a universal IMF, similar to that in the solar neighbourhood. In Cole et al. (2000) and in this paper, we use the form proposed by Kennicutt (1983), which is consistent with the “best estimate” of Scalo (1998):

$$\begin{aligned} dN/d\ln m &\propto m^{-0.4} & (m < 1M_{\odot}) \\ &\propto m^{-1.5} & (m > 1M_{\odot}) \end{aligned} \quad (9)$$

We use the instantaneous recycling approximation to calculate the evolution of the abundance of heavy elements of the cold gas ( $Z_{\text{cold}}$ ) and stars ( $Z_{\star}$ ) in each galaxy, together with that of the hot gas in the halo ( $Z_{\text{hot}}$ ), including the effects of inflows and outflows between the galaxy and halo. The chemical evolution depends on the recycled fraction  $R$  and the yield of heavy elements  $p$ .

**(i) Stellar population synthesis and dust extinction:** In Cole et al. (2000), we calculated the luminosity evolution of each galaxy at different wavelengths using the stellar population synthesis models of Bruzual & Charlot (2000). The effects of dust *extinction* were calculated in a simple way using the dust models of Ferrara et al. (1999), which assume a smooth (unclumped) distribution for both the dust (in a disk) and stars (in a disk and a bulge). In the present paper, we use instead the combined stellar population and dust model GRASIL (Silva et al. 1998) to calculate the galaxy luminosities and spectra including both *extinction* and *emission* by dust. The stellar population part of GRASIL is similar to the Bruzual & Charlot model, as both are based on similar stellar evolution tracks and stellar spectra. The dust part of GRASIL is however considerably more sophisticated than the Ferrara et al. models, in that GRASIL allows for clumping of both dust and stars, and calculates the grain heating and emission as well as the extinction.

The parameters we have chosen for the GALFORM model are the same as those of the standard  $\Lambda$ CDM model of Cole et al. (2000), apart from  $\epsilon_{\star\text{burst}}$  and  $\eta$  describing the timescale and radius of bursts, which were not considered in Cole

et al. . These parameters values are given in Table 1, and were obtained by comparing the model to observations of nearby galaxies, without any consideration of the far-IR or UV properties. We refer the reader to Cole et al. for a complete discussion of the effects of varying the 'old' GALFORM parameters, and for a systematic presentation of the influence of these parameters on the optical-NIR properties of galaxies (LFs, Tully-Fisher relation, disk sizes, morphology, gas content, metallicity, M/L ratios and colours). We only recall here the main observational constraints used to fix each of these parameters:  $\epsilon_{\star\text{disk}}$  - gas fraction of  $L_{\star}$  galaxies;  $\alpha_{\star}$  - variation of gas fraction with luminosity;  $\alpha_{\text{hot}}$  - faint end of LF and Tully-Fisher relation ;  $V_{\text{hot}}$  - faint end of LF and sizes of low- $L$  spirals; IMF - observations of solar neighbourhood;  $\Upsilon - L_{\star}$  in LF;  $p$  - metallicity of  $L_{\star}$  ellipticals;  $f_{\text{ellip}}$  - morphological mix of  $L_{\star}$  galaxies.

Values for  $\epsilon_{\star\text{burst}}$  and  $\eta$  are instead obtained later in this paper by detailed comparison of the results of the combined GALFORM+GRASIL models with observed properties of bursting galaxies.

### 3. The Stellar Population and Dust Model

Far-UV to mm SEDs of model galaxies are calculated using the GRASIL code (Silva et al. 1998), which follows both the evolution of stellar populations and absorption and emission by dust. GRASIL calculates the following: (i) emission from stellar populations; (ii) radiative transfer of starlight through the dust distribution; (iii) heating and thermal equilibrium of dust grains (or thermal fluctuations for small ones); and (iv) emission by dust grains.

#### 3.1. Stellar Population Model

The single stellar population (SSP) libraries included in GRASIL are based on the Padova stellar models and cover a large range in age and metallicity. They include the effects of dusty envelopes around AGB stars (Bressan et al. 1998). The age and metallicity distribution of a composite stellar population is specified by the birthrate function  $\Psi(t, Z)$ , where  $\Psi(t, Z) dt dZ$  gives the mass of stars that were formed in the time interval  $(t, t+dt)$  with metallicities in the range  $(Z, Z + dZ)$ . The SED for the composite stellar population at time  $t$  is

then obtained using

$$L_{\lambda}(t) = \int_0^t dt' \int_0^1 dZ l_{\lambda}(t-t', Z) \Psi(t', Z) \quad (10)$$

where  $l_{\lambda}(\tau, Z)$  is the SED of a SSP of age  $\tau$  and metallicity  $Z$  for the assumed IMF.

For our semi-analytical galaxy formation model,  $\Psi(t, Z)$  is calculated for each galaxy by summing over all the progenitor galaxies which have merged to produce that galaxy, separately for the disk and bulge components. The progenitor galaxies each had their own star formation and chemical history, so that the composite  $\Psi(t, Z)$  obtained in general has a broad distribution of metallicity at each age, i.e. there is no unique age-metallicity relation  $Z(t)$ .

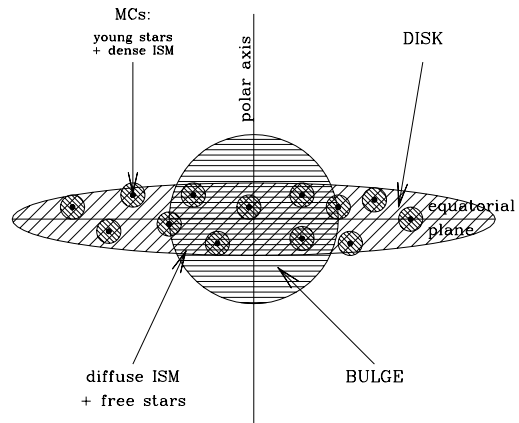


Fig. 1.— Sketch of geometry of stars and dust in the GRASIL model.

#### 3.2. Dust Model

GRASIL computes the radiative transfer of starlight, the heating of dust grains, and the emission from these grains with a self-consistent calculation of the distribution of grain temperatures, for an assumed geometrical distribution of the stars and dust, and a specific grain model. The dust is divided into two components, dense molecular clouds and diffuse cirrus in a disk. Stars form inside clouds and progressively leak out.

Table 2: Adopted values for the adjustable GRASIL parameters. Note that the results depend on the ratio  $M_c/r_c^2$  rather than on the two quantities individually (see § 3.2).

$h_z/h_R(disk)$	0.1
$h_z/h_R(burst)$	0.5
$h_z(dust)/h_z(stars)$	1
$f_{mc}$	0.25
$M_c/r_c^2$	$10^6 M_\odot/(16\text{pc})^2$
$t_{esc}(disk)$	2Myr
$t_{esc}(burst)$	10Myr

The details are given in Silva et al. (1998), but for convenience we summarize the main features here, focusing on the modifications introduced for the purposes of this application. Those GRASIL parameters which are not provided by GALFORM, and are in this sense additional adjustable parameters of the combined GALFORM+GRASIL semi-analytic modelling, are listed in Table 2, together with the adopted values for our standard case. See Fig. 1 for a sketch of the geometry of our model.

**(a) Geometry of stars:** The stars are in two components (Silva et al. (1998) considered only pure disk and pure bulge systems): (i) a spherical bulge with an analytic King model profile,  $\rho \propto (r^2 + r_c^2)^{-3/2}$  for  $r < r_t$ , with concentration parameter  $\log(r_t/r_c) = 2.2$ ; (ii) a disk with a radially and vertically exponential profile, scale-length  $h_R$  and scaleheight  $h_z$ . As described in § 2, the disk and bulge masses,  $M_{disk}$  and  $M_{bulge}$ , and half-mass radii,  $r_{disk}$  and  $r_{bulge}$ , for any galaxy are predicted by the galaxy formation model. The bulge core radius is related to the bulge half-mass radius by  $r_c = r_{bulge}/14.6$ , while the disk scale-length  $h_R$  is related to the disk half-mass radius by  $h_R = r_{disk}/1.68$ . The star formation histories are also calculated separately for the disk and bulge by GALFORM. However, the disk axial ratio  $h_z/h_R$  is a free parameter of the GRASIL model.

As partially anticipated in § 2, in galaxies undergoing bursts, the burst star formation, as well as the gas and dust, are assumed to be in an exponential disk, but with half-mass radius  $r_{burst} = \eta r_{bulge}$  rather than  $r_{disk}$ . The axial ratio  $h_z/h_R$  of the burst region is allowed to be different from

that for disks in non-bursting galaxies. The stars which were formerly in the disks of the galaxies before the galaxy merger which triggered the burst are assumed to become part of the bulge following the merger.

**(b) Geometry of gas and dust:** The gas and dust are in an exponential disk, with the same radial scalelength as the disk stars (either  $r_{disk}$  for normal galaxies or  $r_{burst} = \eta r_{bulge}$  for starbursts), but in general with a different scaleheight, so that  $h_z(dust)/h_z(stars)$  is a free parameter. The gas and dust are in two components within the disk, molecular clouds and the diffuse ISM. The latter corresponds to the cirrus dust. The total gas mass  $M_{cold}$  and its metallicity  $Z_{cold}$  are calculated by the galaxy formation model, but the fraction of the gas in clouds,  $f_{mc}$ , and the cloud mass  $M_c$  and radius  $r_c$  are free parameters of GRASIL, though the results actually depend only on their combination  $M_c/r_c^2$ , which determines, together with the dust/gas ratio (see point (d) below), the optical depth of the clouds (Silva et al. 1998).

**(c) Young stars and molecular clouds:** Stars are assumed to form inside the molecular clouds, and then to escape on a timescale  $t_{esc}$ . Specifically, the fraction of stars still inside clouds at time  $t$  after they formed is assumed to be given by

$$\begin{aligned}
 F(t) &= 1 & (t < t_{esc}) \\
 &= 2 - t/t_{esc} & (t_{esc} < t < 2t_{esc}) \\
 &= 0 & (t > 2t_{esc})
 \end{aligned}
 \tag{11}$$

We allow  $t_{esc}$  to take different values in normal disks and in bursts, in keeping with the results of Silva et al. (1998). Indeed, given the small size scale and the intensity of the star formation activity in bursts, it is conceivable that the star-forming environment is quite different from that in normal spiral galaxies (see also § 3.3).

**(d) Dust grain model:** The dust is assumed to consist of a mixture of graphite and silicate grains and polycyclic aromatic hydrocarbon molecules (PAHs), each with a distribution of grain sizes. Absorption and emission properties are calculated for each grain composition and size. The grain mix and size distribution were chosen by Silva



et al. (1998) to match the extinction and emissivity properties of the local ISM, and are not varied here. The dust/gas ratio  $\delta$  in the clouds and diffuse ISM is assumed to be proportional to the gas metallicity, with a value  $\delta = 1/110$  for  $Z = Z_{\odot} = 0.02$ . Thus, the total dust mass in a galaxy scales as  $M_{\text{dust}} \propto Z_{\text{cold}} M_{\text{cold}}$ .

**(e) Radiative transfer, dust heating and re-emission:** The luminosities of the different stellar components (bulge stars, disk stars, and young stars still in clouds) are calculated using the population synthesis model described above. The GRASIL code then calculates the radiative transfer of the starlight through the dust distribution. Whilst in molecular clouds a full radiative transfer calculation is performed, the effects of scattering by diffuse dust are included only approximately, by assuming that the effective optical depth for absorption is related to the true absorption and scattering optical depths  $\tau_{\text{abs}}$  and  $\tau_{\text{scat}}$  by  $\tau_{\text{abs,eff}} = \sqrt{\tau_{\text{abs}}(\tau_{\text{abs}} + \tau_{\text{scat}})}$ . Thus the dust-attenuated stellar radiation field can be calculated at any point inside or outside the galaxy. Then GRASIL calculates for each point in the galaxy the absorption of radiation, thermal balance and re-emission for each grain composition and size. Thus, the distribution of grain temperatures is calculated self-consistently for the assumed geometry of the stars and dust, including the effects of temperature fluctuations for small grains. The final galaxy SED  $L_{\lambda}$  is obtained by adding the contributions from the starlight (attenuated by dust) and from the dust re-emission, and depends on the inclination angle at which the galaxy is viewed. Emission from dust in the envelopes of AGB stars is included in the SSPs.

Our computations allow us to calculate the amount of energy emitted in the PAH bands, but theoretical predictions of the detailed shapes of the emission features are rather uncertain. Therefore we use the Lorentzian analytical fits to the observed PAH profiles for the Ophiuchus molecular cloud from Boulanger et al. (1998).

### 3.3. Choice of GRASIL adjustable parameters and new GALFORM parameters

The values of GRASIL parameters (Table 2) not provided by GALFORM have been based on a variety of observational data for galaxies in the local universe. For some of them, the choices were made by trying to match model predictions to the observational data, as is discussed in more detail in the relevant sections of this paper. We now summarize the reasons for these choices and for those of the two GALFORM parameters ( $\epsilon_{\star\text{burst}}$  and  $\eta$ ) not considered in Cole et al. (2000)

**(a)  $\epsilon_{\star\text{burst}}$ :** this is chosen mainly so as to reproduce the bright end of the IR luminosity function, which is dominated by bursts triggered by galaxy mergers (§7.4). A secondary (weak) constraint is to reproduce the relation between  $L_{\text{IR}}/L_{\text{UV}}$  and total luminosity or UV slope  $\beta$  observed for starburst nuclei (§6.2). The value controls both the luminosity and lifetime (and thus number density) of starbursts.

**(b)  $\eta = r_{\text{burst}}/r_{\text{bulge}}$ :** the choice of this is mainly based on the observational fact that starburst activity is usually confined to a nuclear region with a size much smaller than the galaxy as a whole, by about one order of magnitude (e.g. Sanders & Mirabel 1996, and references therein). For instance, in Arp 220 most of the molecular gas is found in the central  $\sim 300\text{pc}$  (Scoville et al. 1997), and the mid-IR light is dominated by more or less the same region (Keto et al. 1992), while the half-light radius for the old stellar population is  $\sim 3\text{kpc}$  (Wright et al. 1990). The value of  $\eta$  controls the amount of extinction of starlight from bursts by the diffuse ISM, which however is usually overwhelmed (in bursts) by extinction in molecular clouds (see §6.4). Therefore our results are not very sensitive to the precise choice of this parameter, nor to the value of  $h_z/h_R$  in starbursts (discussed below).

**(c)  $h_z/h_R$ :** for normal disks, we choose a value of 0.1, consistent with observations of the stellar light distributions in edge-on spiral galaxies (e.g. Xilouris et al. 1999). It is also the typical value used by Silva et al. (1998) to fit the

SEDs of spiral galaxies. This value is also important, and the adopted value turns out to be suitable, to match the observed difference in extinction between spiral galaxies seen edge-on and face-on (§5.2). Apart from this test, most predicted properties are not very sensitive to  $h_z/h_R$ . The choice of  $h_z/h_R = 0.5$  for starbursts is based on general observational indications that they are only moderately flattened.

**(d)  $h_z(dust)/h_z(stars)$ :** this parameter has a significant effect on how much starlight is absorbed in the diffuse medium. From observations of our own galaxy it is known that the scaleheight of stars increases with the age of the stellar population, so that there is no unique value for  $h_z(dust)/h_z(stars)$ . The scaleheight of the gas is comparable to that of the youngest stars. Since we are particularly interested in having a realistic estimate of the extinction in the UV, both because it is strongest there and because this is an important source for dust heating, we choose  $h_z(dust)/h_z(stars) = 1$  to match what is seen for the young stars.

**(e)  $f_{mc}$ :** this can be estimated observationally from the ratio of molecular to atomic hydrogen in galaxies, since in normal spiral galaxies most of the hydrogen in molecular clouds is in  $H_2$ , while most of the intercloud medium is atomic  $HI$ . Our adopted  $f_{mc}$  implies a ratio  $H_2/HI$  similar to the typical one for  $L_*$  spirals found by Sage (1993). Larger values reduce the extinction in the diffuse ISM and produce a somewhat colder molecular clouds emission, but our results are in general not significantly affected as long as we keep  $f_{mc}$  in the range 0.2–0.8.

**(f)  $M_c, r_c$  :** as already remarked (§ 3.2) the predicted SEDs depend on the ratio  $M_c/r_c^2$ , rather than  $M_c$  and  $r_c$  separately. Thus  $M_c$  has been chosen to match typical giant molecular clouds in our own and nearby galaxies, while  $r_c$  is chosen based on the results of Silva et al. (1998), who tuned  $M_c/r_c^2$  to fit the SEDs of starburst galaxies in particular. The resulting value for  $r_c$  is consistent with direct measurements of cloud radii.

**(g)  $t_{esc}$ :** this is a very important parameter in the model, since it is this that mainly controls how much of the radiation from young stellar populations is absorbed by dust. Silva et al. (1998) found from detailed fits to 3 nearby spirals values of 2.5, 3 and 8 Myr. For normal spirals, we favor a value of 2 Myr, close to the lower limit of this range, rather than the average 5 Myr. Although the latter provides an equally good overall fit to the LFs (somewhat better for IRAS colors and LFs, § 7.4, but somewhat worse for the UV LF), the former is more consistent with the massive star census in our own and nearby galaxies, which suggests that the time for which the stars are obscured by dust is about the 20 % of the total lifetime for the brightest stars, above say  $30 M_\odot$ , whose lifetime is around 6 Myr. For starbursts, the value we choose is based mainly on the comparison with properties of UV-bright starbursts in §6.2. This leads us to a value closer to that of normal spirals than the values  $t_{esc} = 20\text{--}60$  Myr found by Silva et al. (1998) from fitting 3 nearby starbursts, and suggests that the starburst galaxies used by Silva et al. may be not representative of the whole population. The difference could also be due in part to the more complex geometry adopted in this paper for starburst galaxies.

#### 4. Generation of model galaxy catalogues

The GALFORM model is run for a set of dark matter halos covering a large range in mass, and generates a catalogue of model galaxies, including information about the following properties for each galaxy at the chosen epoch: stellar masses  $M_{\text{disk}}$ ,  $M_{\text{bulge}}$ , and half mass radii  $r_{\text{disk}}$  and  $r_{\text{bulge}}$  of the disk and bulge, mass  $M_{\text{cold}}$  and metallicity  $Z_{\text{cold}}$  of gas in the disk, and the star formation histories  $\Psi(t, Z)$  of the disk and bulge separately, including both star formation in disks and during bursts, and specifying the metallicity distribution of the stars of each age. In addition, each galaxy has a weight or number density  $n$ , such that that galaxy should appear  $N = nV$  times in an average volume of the universe  $V$ .

The GALFORM code outputs all the galaxies for each different halo that is calculated, down to a minimum mass controlled by the mass resolution of the merger tree. In practice, this means that the model catalogue contains many more low mass galaxies than high mass galaxies. Running the GRASIL code on every galaxy in the original catalogue is neither feasible (because of computer time) nor necessary. We therefore select a subset of galaxies from the catalogue chosen to sample galaxies more evenly in mass, and redistribute the weights to give the same total number density in each mass range. The GRASIL code is then run on each galaxy in this reduced catalogue to give the SED  $L_\lambda$  including both stellar emission and dust absorption and emission, and statistical properties (e.g. luminosity functions) are then calculated making use of these weights. In fact, we calculate 2 samples of galaxies, a “normal” sample and a “burst” sample, as follows:

(a) *Normal galaxies:* By “normal” galaxies, we here simply mean galaxies not selected to have had a recent burst. From the parent GALFORM catalogue, we select a sample with equal numbers of galaxies in equal bins in  $\log M_*$ ,  $M_*$  being the total stellar mass of the galaxy. Within each mass bin, galaxies are randomly selected (allowing for multiple selection of the same galaxy) with probability proportional to their weight  $n$ . The selected galaxies are then assigned new weights  $n_i$ , such that each galaxy within the same bin has the same weight (multiply selected galaxies being counted as separate objects), and that the sum of the weights (i.e. number densities) within a bin is the same as in the parent catalogue. We have used bins with  $\Delta \log M_* = 0.3$  and about 40 galaxies per bin.

(b) *Burst galaxies:* By “burst” galaxies we mean galaxies which have had a burst in the recent past, at whatever redshift we are looking. Bursts have short durations compared to the age of the universe, so the fraction of galaxies undergoing a burst at any one time is very small, but they can be very luminous, and so may dominate the galaxy luminosity function at the highest luminosities. In practice, our “normal galaxy” catalogue contains too few galaxies in total to provide a representative sample of galaxies seen during their burst phase. Rather than use a greatly enlarged “normal galaxy” sample, it is more efficient to calcu-

late a separate sample of “burst” galaxies, as follows: for a redshift  $z$ , we choose a subsample of galaxies which have had bursts during the time interval  $t(z) > t > t(z) - T$ , where  $t(z)$  is the age of the universe at redshift  $z$ , with equal numbers of galaxies in equal bins in  $\log M_{\text{burst}}$ ,  $M_{\text{burst}}$  being the mass of stars formed in the most recent burst. The galaxies are assigned new weights  $n_i$  analogously to the case of normal galaxies, but now conserving the total number density in bins of  $M_{\text{burst}}$  for the galaxies which have had bursts more recently than  $T$ . For each burst galaxy, we then run GRASIL to calculate the total galaxy luminosity at a set of times after the start of the burst, chosen to sample all phases of the burst evolution, including the highest luminosity phase of short duration. If  $T \ll t(z)$ , then the rate of bursts per unit volume during the time interval  $T$  can be taken as constant. Then, for the  $i$ th galaxy in the  $j$ th phase in the burst evolution that lasts a time  $\Delta t_j$ , the number density of galaxies that should be found in this phase is

$$n_{ij} = n_i \left( \frac{\Delta t_j}{T} \right) \quad (12)$$

These weights can then be used to calculate statistical properties such as luminosity functions. When combining the “normal” and “burst” galaxy samples, the normal galaxies with bursts more recent than  $T$  are explicitly excluded, to avoid statistical double-counting. In practice, we chose  $T = t(z)/20$  at all  $z$ , with bins  $\Delta \log M_{\text{burst}} = 0.3$ , around 10 galaxies per bin, and around 10 output times per galaxy, for  $0 < t - t_{\text{burst}} \lesssim 100\tau_e$ . For many calculations of statistical distributions, we then interpolate between these output times to have more burst phases.

## 5. Properties of spiral galaxies

In this section, we test the model predictions for disk galaxies against observed emission and absorption properties of nearby spirals.

### 5.1. SEDs of face-on spirals

We compared the predicted near-UV to far-IR SEDs of our model galaxies with the broad-band SEDs of a complete sample of nearby spiral galaxies (de Jong & van der Kruit 1994), consisting of a diameter-limited sample of 86 nearly face-on,

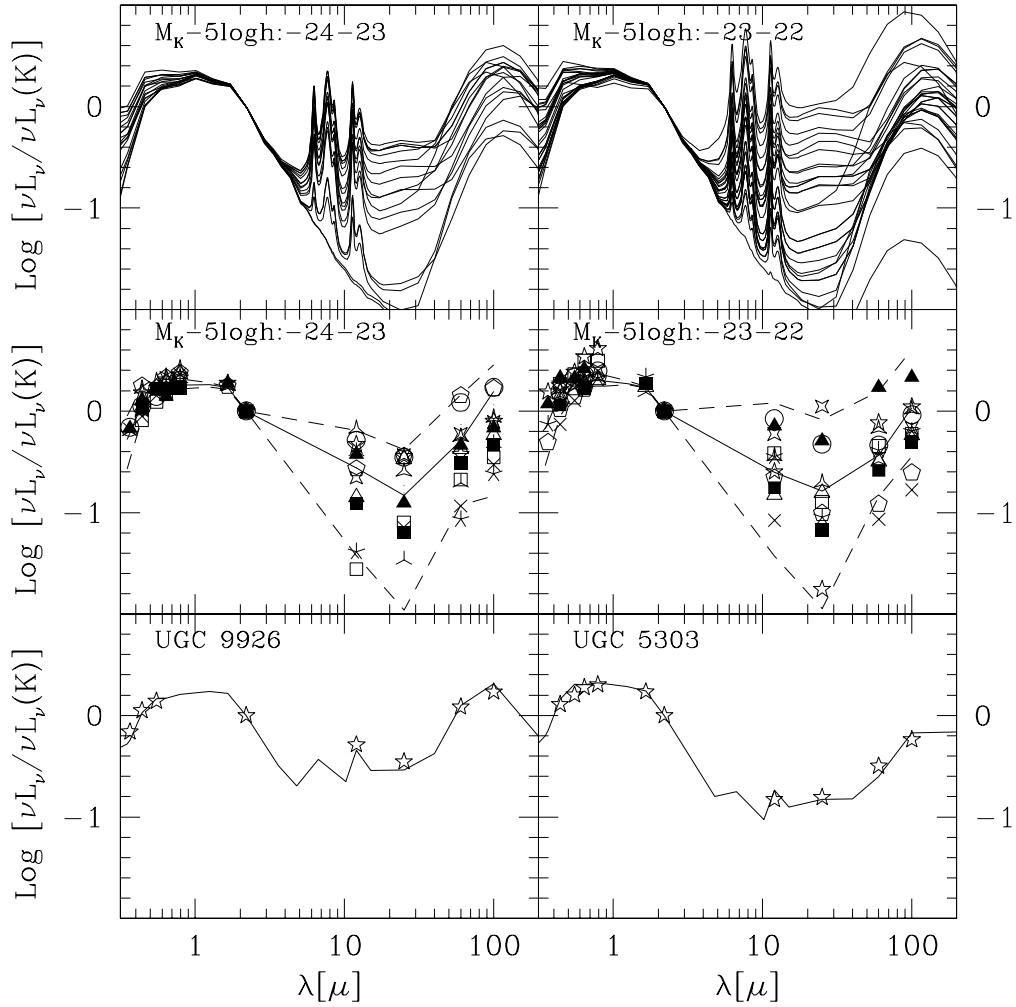


Fig. 2.— Upper panels: SEDs (normalized to the K-band) of a representative sample of spiral galaxies from the models. Middle panels: Comparison of the models with the observed SEDs of a sample of face-on spiral galaxies obtained by de Jong & van der Kruit (1994). The median and the 10% and 90% percentiles of the model SEDs are plotted as lines. Lower panel: comparisons between observed SEDs of individual galaxies from the sample and selected model SEDs. The left-hand panels are for galaxies in the luminosity range  $-23 > M_K - 5 \log h > -24$ , and the right-hand panels for  $-22 > M_K - 5 \log h > -23$ .

disk-dominated galaxies. de Jong & van der Kruit measured fluxes of these galaxies in the BVRIHK bands. We have supplemented these with U-band magnitudes from the literature and IRAS 12, 25, 60, 100 $\mu\text{m}$  fluxes from Saunders (1997).

We considered only those model galaxies with bulge to total light ratio  $B/T \leq 0.5$  in the B-band, corresponding to the range of types in the de Jong sample (e.g. Simien & de Vaucouleurs 1986). From Figure 2 it is apparent that the models reproduce the observed spectral trends reasonably well. This is particularly impressive since the ratio between the infrared and the optical-UV spans more than one order of magnitude, both in the observed and in the theoretical SEDs. The predicted infrared emission peaks at wavelengths somewhat larger than those sampled by IRAS, in agreement with recent ISO observations (e.g. Alton et al. 1998). The emission in the mid-infrared is dominated by PAH molecular bands.

Figure 3 shows the effects on typical SEDs of factor 2 variations in the molecular cloud fraction  $f_{mc}$ , their mass  $M_c$  (i.e. their optical depth, having fixed the radius) and the escape timescale  $t_{esc}$ . The effects are mostly confined to the mid-IR between 8 and 40  $\mu\text{m}$  and in the UV below 0.4  $\mu\text{m}$ . In these spectral regions, the predicted flux may change by up to a factor  $\sim 2$ , while the effects are almost negligible elsewhere. In the mid-IR the most important parameter is the cloud optical depth, while in the UV the effects of  $t_{esc}$  dominate.

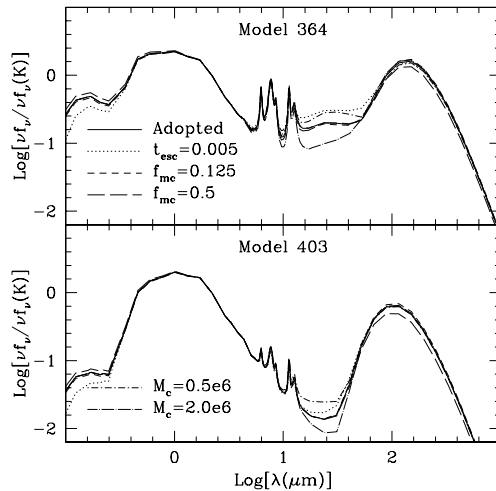


Fig. 3.— Effects on typical SEDs of factor 2 variations of  $f_{mc}$ ,  $M_c$  (effectively, the cloud optical depth) and  $t_{esc}$ . In each case only one parameter is varied with respect to the standard model.

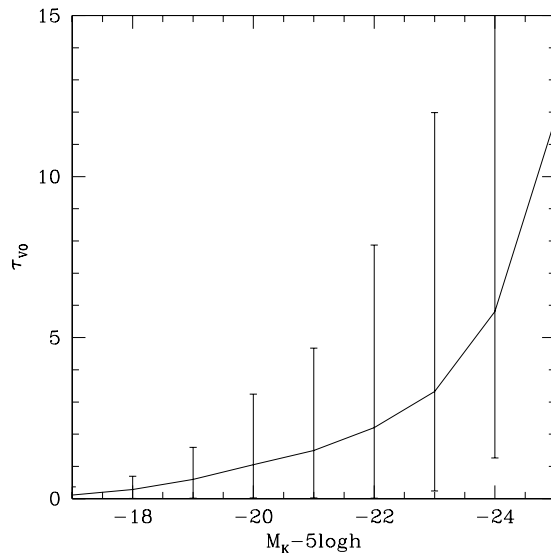


Fig. 4.— Predicted dependence of dust optical depth on luminosity for spiral galaxies in the model.  $\tau_{V0}$  is the central face-on extinction optical depth in the V-band for the diffuse dust component in the disk. The line shows the median, and the error bars show the 10% and 90% percentiles. Model galaxies are selected to have  $B/T < 0.4$  in the B-band.

## 5.2. The global extinction in spiral galaxies

The models predict that the extinction in galaxy disks should increase strongly with galaxy luminosity, as shown in Figure 4. Clearly, in comparing predictions of dust extinction with observations, one must be careful to specify the luminosity of the objects concerned.

There have been many attempts to measure or observationally constrain the total dust extinction in galaxy disks, using a variety of techniques: the inclination dependence of magnitudes or colours (e.g. de Vaucouleurs et al. 1991; Giovanelli et al. 1995), surface brightness distributions in edge-on galaxies (e.g. Kylafis & Bahcall 1987), colour gradients in face-on disks (e.g. de Jong 1996c), and the ratio of far-IR to UV luminosities (e.g. Xu & Buat 1995; Buat & Xu 1996; Wang & Heckman 1996). In general, different techniques have given somewhat different answers.

Xilouris et al. (1999) estimate dust extinctions by fitting detailed models of the star and dust distributions to the observed surface brightness distributions of edge-on spiral galaxies. Their dust models include scattering. From their six Sb-Sc spirals with luminosities in the range  $-17.5 > M_B - 5 \log h > -19.0$ , we obtain a median central face-on extinction optical depth  $\tau_{V0} = 0.6$ . In comparison, for edge-on galaxies in our model in the same luminosity range (after extinction), and with  $0.1 < B/T < 0.3$  in the B-band, we find a median value  $\tau_{V0} = 2.2$ , which is significantly larger. There could be several reasons for this difference between the models and the observations: there may be a problem with the Xilouris et al. method for deriving  $\tau_{V0}$  from the observations, or the Xilouris et al. sample may not be representative, or the problem might be with our assumption that the dust and stars have the same exponential scalelength. The extinction-inclination observational test discussed next implies extinctions for edge-on galaxies in this luminosity range which are at least as large as those predicted by our model.

We considered the dependence of the net extinction on the inclination angle at which a galaxy is viewed. This has been studied in many papers using different methods, most recently by Tully et al. (1998), who also summarize the results from the earlier studies. Tully et al. mea-

sure the dependence of  $B - K$ ,  $R - K$  and  $I - K$  colours on galaxy inclination at a given K-band luminosity, the K-band being chosen to minimize extinction effects. They have a complete sample of spirals covering a large range in luminosity,  $-18.5 \gtrsim M_K - 5 \log h \gtrsim -24.5$ . They find a strong luminosity dependence, with a difference in B-band extinction between edge-on and face-on galaxies of about 2 mag for the brightest galaxies, and negligible for the faintest ones.

Tully et al. (1998) follow the usual practice and parameterize the extinction relative to that for the galaxy seen face-on as

$$A_\lambda^{i-0} \equiv m_\lambda(i) - m_\lambda(0) = \gamma_\lambda \log(a/b) \quad (13)$$

where  $\gamma_\lambda$  is a function of the passband. The axial ratio  $a/b$  is assumed to be related to the inclination angle  $i$  by

$$\cos i = \sqrt{\frac{(b/a)^2 - q^2}{1 - q^2}} \quad (14)$$

where  $i = 0$  for a face-on system, and  $q$  is the axial ratio of a galaxy seen edge-on.

The models are compared with observations in Fig. 5. We use equation (14) to convert from the model inclination angle to the axial ratio, assuming  $q = 0.1$ , which is the ratio  $h_z/h_R$  adopted in our galaxy models. We considered model galaxies corresponding to the morphological types Sa-Scd, and four ranges in K-band luminosity, corresponding to the ranges chosen by Tully et al. (1998), indicated by the different symbols in the figure.

The three lines in the figure correspond to different values of the slope  $\gamma_B$ . The model galaxies approximately follow the linear dependence on  $\log(a/b)$  (equation (13)), but with slopes  $\gamma_B$  that are somewhat shallower, at any given luminosity, than those observationally inferred by Tully et al. (1998). For instance, for the luminosity range  $-23.0 < M_K - 5 \log h < -22.0$ , our models follow an average slope  $\langle \gamma_B \rangle \approx 0.9$ , while Tully et al. find  $\gamma_B = 1.1 \pm 0.5$ , after allowing for the K-band extinction. The slope predicted by our models depends on the value chosen for the parameter  $h_z/h_R$  (see also § 3.3). We have checked that increasing  $h_z/h_R$  from our adopted value of 0.1 decreases the slope, while reducing it does not increase the slope significantly.

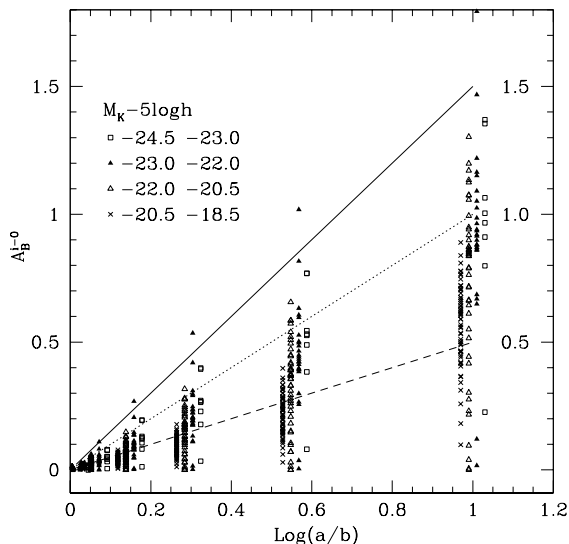


Fig. 5.— Dependence of extinction on inclination angle predicted by our galaxy models. The quantity  $A_B^{i=0} = M_B(i) - M_B(0)$  is plotted against the apparent axial ratio  $a/b$ , for the Sa-Scd models (with  $0.04 < B/T < 0.4$  in the B-band). The galaxies are plotted with different symbols in four K-band luminosity ranges, as detailed in the figure. The same galaxies are plotted seen at different inclinations. For clarity, small horizontal offsets have been applied to the galaxies in different luminosity ranges. Three lines are plotted corresponding to equation (13) with the slopes  $\gamma_B = 0.5, 1$  and  $1.5$ .

The agreement for the inclination test is anyway acceptable. Part of the discrepancy could be due to our simplified treatment of scattering by the diffuse dust (§ 3.2). In our models, the absolute extinction is often dominated by the molecular clouds, but the difference between the face-on and the edge-on extinction is entirely due to the cirrus. Comparisons of our model with that of Ferrara et al. (1999), where the treatment of scattering is more accurate, show that for the brightest objects this effect can account for about 0.1-0.2 mag of the differential extinction in the B band.

## 6. Properties of starburst galaxies

Starburst galaxies are broadly defined as galaxies in which the current star formation rate is much

greater than its time-averaged value, and the star formation timescale correspondingly much shorter than the age of the universe. This definition includes objects with a wide range of properties, from bursting dwarf irregular galaxies (e.g. Thuan & Martin 1981) to the ultra-luminous IR galaxies (ULIGs) found by IRAS (e.g. Sanders & Mirabel 1996). In practice, a large variety of observational criteria have been applied to select samples of starburst galaxies, ranging from optical morphologies and spectra (e.g. Balzano 1983) to IR colours and luminosities (e.g. Armus et al. 1990; Lehnert & Heckman 1995). In our galaxy formation model, bursts are assumed to occur following major mergers of galaxies, producing elliptical galaxies from disk galaxies. For the ultra-luminous IR galaxies, the link between the starburst activity and galaxy mergers is clearly established (e.g. Sanders & Mirabel 1996), while for low-luminosity starbursts, additional triggering mechanisms probably operate, which are not included in our model. In this section we will compare the properties of starbursts predicted by our model with those of various observational samples.

## 6.1. Properties of starbursts in the model

Figure 6 shows how various properties of the bursts in our model vary with the stellar mass of the galaxy,  $M_{\text{star}}$ , after completion of the burst. The total mass of new stars formed in the burst,  $M_{\text{burst}}$ , is seen to increase with the galaxy mass, with the fraction of stars formed in the burst being typically between  $\sim 1\%$  and  $\sim 50\%$ . An exception to this trend is the group of points in the lower right corner of Fig.6a corresponding to small bursts occurring in large galaxies. These small bursts are produced by mergers between gas-poor elliptical galaxies. The main trend in panel (a) is produced by mergers between disk galaxies containing significant fractions of gas, and these dominate the statistics at all burst masses. The star formation rate during the burst is  $(M_{\text{burst}}/\tau_e)\exp(-t/\tau_e)$ , with  $t$  measured from the start of the burst. The peak star formation rate is thus  $M_{\text{burst}}/\tau_e$ , and occurs at the beginning of the burst. This peak SFR is seen also to increase with the host galaxy mass. The half-mass radius  $r_{\text{burst}}$  and exponential decay time  $\tau_e$  of the burst are assumed to scale with the half-mass radius and dynamical timescale of the host galaxy, and also increase with galaxy mass. Large bursts, with  $M_{\text{burst}} \sim 10^{10}h^{-1}M_{\odot}$ , are predicted to occur in galaxies with  $M_{\text{star}} \sim 10^{11}M_{\odot}$ , and to have radii  $r_{\text{burst}} \sim 0.5h^{-1}\text{kpc}$ , star formation timescales  $\tau_e \sim 5 \times 10^7\text{yr}$ , and peak star formation rates  $\sim 200h^{-1}M_{\odot}\text{yr}^{-1}$ . These are similar properties to those inferred observationally for the ULIGS (e.g. Sanders & Mirabel 1996).

## 6.2. Properties of UV-bright starbursts

A large amount of work has been done on samples of UV-bright starbursts selected from the catalogue of UV spectra of star-forming galaxies of Kinney et al. (1993). Various correlations have been found, for instance between the bolometric luminosity, the UV/IR ratio, the slope of the UV continuum and the metallicity (e.g. Meurer et al. 1995; Heckman et al. 1998). In this section, we compare the properties of our model starbursts with some of this observational data.

The observational sample that we use for our comparison is that of Heckman et al. (1998), who selected 45 starburst and star-forming galaxies from the original atlas of Kinney et al. . The

criteria for a starburst galaxy to appear in the Kinney et al. catalogue are (a) that it has been previously classified as a starburst based on optical data, usually meaning that it has a compact optical morphology and strong optical emission lines (but no AGN activity) (e.g. Balzano 1983); and (b) that it has been observed by IUE and has a high enough surface brightness within the IUE aperture to produce a reasonable quality UV spectrum. The catalogue is not in any sense statistically complete. The starburst activity in these galaxies is generally confined to the central regions. (The galaxies have mostly been selected so that the starburst activity fits within the IUE aperture,  $20'' \times 10''$ , while the optical diameters of the underlying galaxies are typically a few arcminutes.)

For the galaxies in their sample, Heckman et al. (1998) measured a UV luminosity  $L_{UV} \equiv \lambda L_{\lambda}(1900\text{\AA})$  and mean continuum slope  $\beta$  between 1250 and 1850  $\text{\AA}$  (defined by  $L_{\lambda} \propto \lambda^{\beta}$ ) from IUE spectra, and a far-IR luminosity  $L_{FIR}$  from IRAS measurements. Heckman et al. use the definition of  $L_{FIR}$  from Helou et al. (1988), which can be expressed as in terms of the luminosities in the 60 and 100  $\mu\text{m}$  IRAS bands as

$$L_{FIR} = 0.65\nu L_{\nu}(60) + 0.42\nu L_{\nu}(100) \quad (15)$$

$L_{FIR}$  provides an estimate of the 40 – 120  $\mu\text{m}$  luminosity. The quantity  $L_{FIR} + L_{UV}$  is similar to the bolometric luminosity in the case of starbursts, where most of the radiation is emitted in either the UV or the FIR. The galaxies in the Heckman et al. sample cover the range  $L_{FIR} + L_{UV} \sim 10^8 - 10^{11}L_{\odot}$ .

The evolutionary tracks of a selection of model starbursts, with burst masses covering the range  $M_{\text{burst}} \sim 10^7 - 10^{10}M_{\odot}$ , in  $L_{FIR} + L_{UV}$ ,  $L_{FIR}/L_{UV}$  and  $\beta$  are shown in Figure 7, together with observational data for the Heckman et al. sample. We have calculated these quantities from the model SEDs to match the way they are calculated from the observational data. The bolometric luminosities of the model bursts, as measured by  $L_{FIR} + L_{UV}$ , peak soon after the start of the burst, following which they evolve towards smaller values. At the same time, the amount of dust reprocessing of the radiation, as measured by  $L_{FIR}/L_{UV}$ , also decreases. This results from two effects: the escape of young stars from the dense



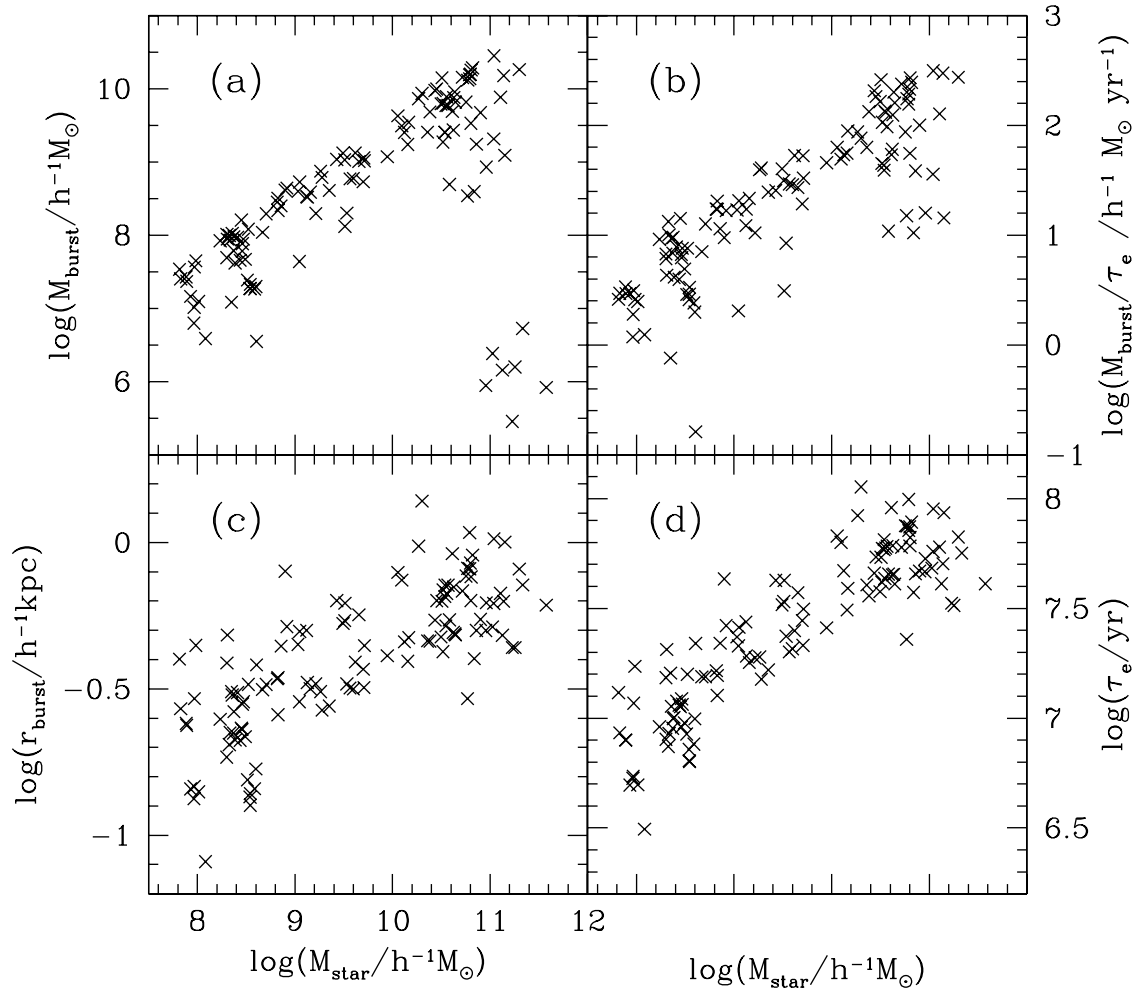


Fig. 6.— Properties of starbursts in the model at  $z = 0$ . (a) The mass of new stars formed in the burst,  $M_{\text{burst}}$  vs the stellar mass of the galaxy after the burst,  $M_{\text{star}}$ . (b) The peak star formation rate in the burst  $M_{\text{burst}}/\tau_e$  vs  $M_{\text{star}}$ . (c) The half-mass radius of the burst  $r_{\text{burst}}$  vs  $M_{\text{star}}$ . (d) The exponential decay time of the burst  $\tau_e$  vs  $M_{\text{star}}$ .

molecular clouds, and the decrease in the optical depth of the diffuse dust component as the gas in the burst is consumed. The UV slope  $\beta$  initially evolves towards more negative values, i.e. *bluer*, as the net dust opacity falls. However, as the rate of formation of new stars drops and the dominant stellar population becomes older, the *intrinsic* unabsorbed stellar spectrum becomes redder, so the

evolution in  $\beta$  reverses, the models becoming redder with time even though the dust attenuation is falling. This happens after 20 – 30 Myr, controlled mainly by the stellar evolution timescale. As long as the evolution in  $\beta$  is dominated by the declining dust opacity, the models stay close to the locus of observed points in the  $L_{\text{FIR}} + L_{\text{UV}}$  vs  $L_{\text{FIR}}/L_{\text{UV}}$  and  $L_{\text{FIR}}/L_{\text{UV}}$  vs  $\beta$  panels, but when

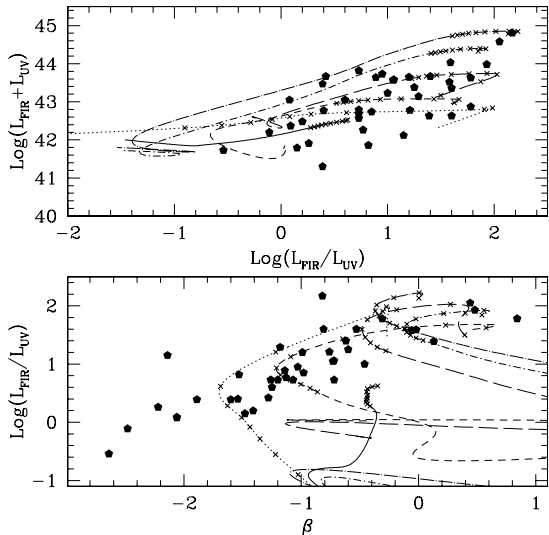


Fig. 7.— Upper panel:  $L_{FIR} + L_{UV}$  (roughly corresponding to the bolometric luminosity) in  $h^{-2}\text{ergs}^{-1}$  versus the ratio of the IR to the UV luminosity  $L_{FIR}/L_{UV}$ . Lower panel: the relation between  $L_{FIR}/L_{UV}$  and the slope  $\beta$  of the UV continuum. In each panel, the filled symbols show observed local starbursts from Heckman et al. (1998), while the lines show the evolutionary tracks of five different model starbursts. The bursts start towards the upper right part of each panel, and evolve towards the lower left (top panel) or lower right (bottom panel). The crosses mark the age since the start of the burst in steps of 5 Myr.

the intrinsic stellar spectrum starts to redden with age, the models move away from the observed locus. This is not in itself in contradiction with observations, since there are selection effects in the observational sample, as we discuss below.

The burst evolution involves the interplay between two timescales, the lifetime of massive stars,  $\sim 10^7\text{yr}$ , and the exponential decay time  $\tau_e$  of the star formation rate and gas mass in the burst. The latter varies with burst mass, being larger than the stellar evolution timescale for large bursts, and comparable for small bursts, as shown in Fig 6. The model starbursts begin their evolution with a large infrared excess and a flat UV slope (upper and lower panel of Fig. 7). Fainter bursts, which

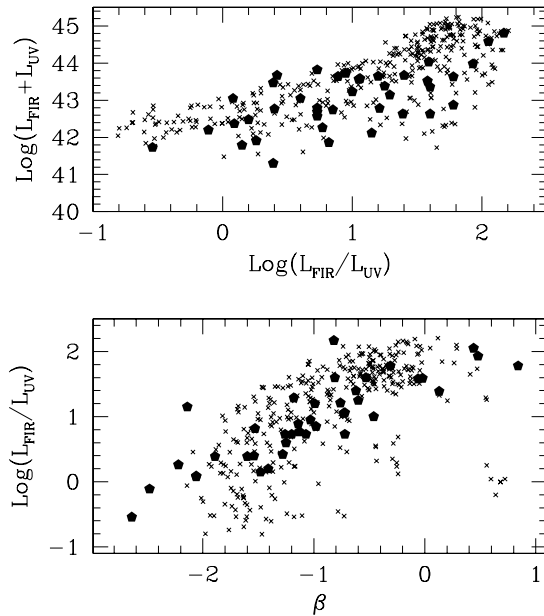


Fig. 8.— Same as in Fig. 7 but for a random sample of model starbursts (crosses), as described in the text. The filled pentagons are the same observational data from Heckman et al. (1998).

have lower gas column densities and are on average also more metal poor, quickly exhaust their gas content and evolve toward a low infrared excess and a negative UV slope, along the locus defined by observations (lower panel of Fig.7). Conversely, brighter bursts, having larger gas column densities and higher metallicities, remain highly enshrouded by dust until, after a few tens of Myr, the dominant stellar population has become intrinsically old. Their UV continuum slopes always remain flat, at the beginning because of reddening and at later times because of age.

In summary, the model starbursts lie close to the region occupied by observed bursts in Fig. 7 as long as the stellar population is young, in the sense of the UV light being dominated by very massive stars. The position of bursts along the observational locus is then determined mostly by the net dust opacity in the UV, in agreement with the interpretation of Meurer et al. (1995) and Heckman et al. (1998). This in turn depends both on the initial gas mass, radius and metallicity of the burst, and on its evolutionary stage.

A detailed comparison with the Heckman et al. observations would require us to construct a mock catalogue of model starbursts obeying the same selection criteria as the observed sample. Unfortunately, the observational selection criteria are rather ill-defined. In addition, one of the selection criteria is the presence of strong *HII* region emission lines, and the GRASIL code at present does not calculate these emission line properties. Instead, we simply select starbursts with ages since the start of the burst less than  $t_{max}$ , to account roughly for the effect that as soon as most of the massive stars have evolved away, the galaxy will no longer produce strong emission lines, and so no longer be classified as a burst in the observational sample. Fig. 8 shows the resulting distribution of points for the choice  $t_{max} = 50\text{Myr}$ . The model starbursts are seen to follow similar relations to the observational sample. The results do not depend sensitively on the choice of  $t_{max}$ .

Several parameters may in principle affect the spectral properties of a model starburst galaxy and therefore the location of our models in the above plots, but the most critical are the ratio between the star formation timescale and the dynamical time ( $\epsilon_{\starburst}^{-1} = \tau_{\starburst}/\tau_{bulge}$ ), and the escape time ( $t_{esc}$ ) for newly born stars to escape from their parental clouds. The former affects the bolometric luminosity, which is almost directly proportional to the star formation rate, and thus inversely proportional to the star formation timescale. The latter affects the fraction of light absorbed inside clouds, and so may affect both the slope of the UV spectrum and the ratio between the IR and UV luminosities. The distribution of model points in Fig. 8 can therefore be used to constrain the values of  $\epsilon_{\starburst}$  and  $t_{esc}$ . However, we found that changes in either of these parameters by a factor  $\sim 2$  either way would only slightly worsen the match with observations.

### 6.3. Infrared colours

We now consider the infra-red and sub-mm colours of starbursts and normal galaxies. Figure 9 shows the dependence of the mean IRAS colours on infra-red luminosity. This plot includes all model galaxies, both normal and starbursts. Their IRAS band luminosities are calculated by convolving the SEDs with the IRAS response functions. In calculating the mean colours, the models

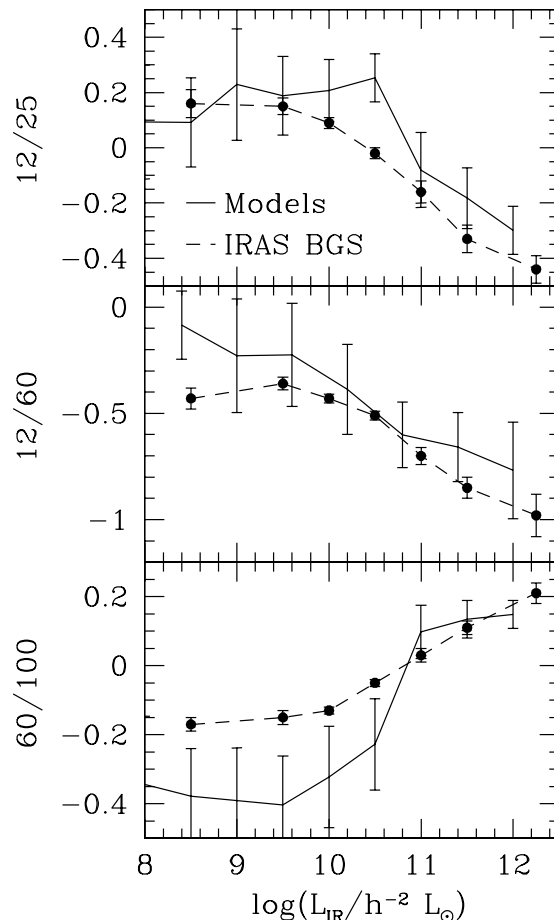


Fig. 9.— Infra-red colours versus total infra-red luminosity. The three panels show the 12/25, 12/60 and 60/100  $\mu\text{m}$  colours respectively, defined as the log of the ratio of  $\nu L_\nu$  in each band. In each panel, the solid line with error bars shows the mean and dispersion from the models, while the dashed line with error bars shows the mean and error on the mean measured by Soifer & Neugebauer (1991) from the IRAS Bright Galaxy Survey.

are weighted by their number density and by a factor  $L_\nu^{3/2}(60\mu\text{m})$  to account approximately for the volume within which a galaxy would be visible in a 60 $\mu\text{m}$  flux-limited sample.  $L_{IR}$  is the standard estimate of the total 8 – 1000 $\mu\text{m}$  IR luminosity from the luminosities in the four IRAS bandpasses

(Sanders & Mirabel 1996):

$$L_{IR} = 0.97\nu L_\nu(12) + 0.77\nu L_\nu(25) + 0.93\nu L_\nu(60) + 0.60\nu L_\nu(100). \quad (16)$$

The model predictions are compared with the observed mean colours calculated by Soifer & Neugebauer (1991) from the IRAS bright galaxy sample (IRAS BGS, Soifer et al. 1989), which is a complete sample flux-limited at  $60\mu\text{m}$ . Models and observations, in particular the  $12/60\mu\text{m}$  colour, show in general similar trends.

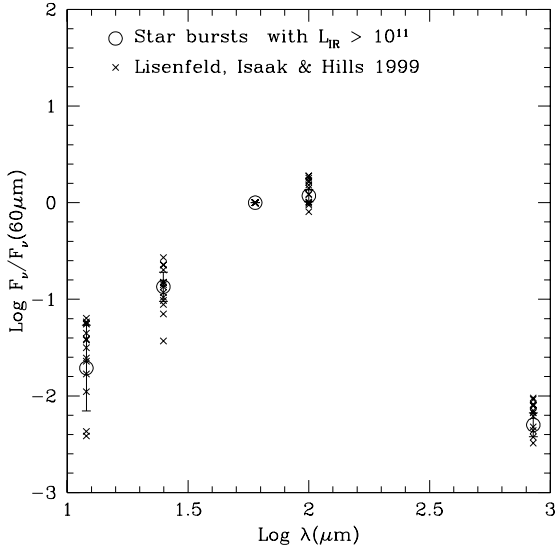


Fig. 10.— Average SED of model starbursts with  $L_{IR} \geq 10^{11} h^{-2} L_\odot$  (empty circles) compared to the observational data (crosses) for 14 luminous starbursts from Lisenfeld et al. (2000). (We exclude galaxies with only upper limits at  $850\mu\text{m}$ .) All SEDs are normalized to the  $60\mu\text{m}$  luminosity. The error bars show the dispersion in the models.

Figure 10 shows the quite good agreement between the average IR and sub-mm SED of model starburst galaxies, and the observed SEDs of luminous infra-red galaxies from the sample of Lisenfeld et al. (2000). The limit  $L_{IR} \geq 10^{11} h^{-2} L_\odot$  for the models has been chosen to approximately reproduce the selection for the Lisenfeld et al. sample. Note that the dust opacity in our models decreases as  $\lambda^{-b}$  with  $b \approx 2$  for  $100 \lesssim \lambda \lesssim 1000\mu\text{m}$ , while Lisenfeld et al. , by fitting optically thin single temperature models to the data at  $\lambda \geq 60\mu\text{m}$ ,

derived  $b$  values in the range 1.5–2. Our models demonstrate that the shallower slopes can instead be explained by the distribution of dust temperatures within each galaxy.

#### 6.4. Extinction in starburst galaxies

An important problem in the study of star-forming galaxies is to determine the amount of attenuation of starlight by dust, especially in the UV. This bears directly on the determination of star formation rates in galaxies from their UV luminosities. For our own and a few nearby galaxies, the *extinction* law of the dust can be measured directly from observations of background stars, where the dust acts as a foreground screen. The differences found between the shapes of the extinction curves of the Galaxy, the Large Magellanic Cloud and the Small Magellanic Cloud below  $\lambda \leq 2600\text{\AA}$  (e.g. Fitzpatrick 1989) are often ascribed to the different metallicities in these systems, covering the range  $Z \sim 0.1 - 1 Z_\odot$ . Recently, Calzetti et al. (1994) (see also Calzetti 1997, 1999) have analyzed the dust extinction in starburst galaxies. In this case, the measurement of the extinction is more complicated, since one measures the integrated light of the whole system, where stars and dust are mixed in a complex way. From the optical and UV spectra of a sample of UV-bright starbursts, Calzetti et al. derive an average *attenuation law* characterized by a shallower far-UV slope than that of the Milky Way extinction law, and by the absence of the  $2175\text{\AA}$  feature. This is at first sight quite surprising, because the metallicities of these galaxies are mostly similar to that of the Milky Way, and so they might be expected to have similar dust properties. The question is then to what degree the differences between the starburst attenuation law and the Milky Way extinction law are due to the geometry of the stars and dust, and to what degree they can only be explained by differences in dust properties.

Figure 11 compares the average attenuation curves for galaxies from our model with the empirical “attenuation law” obtained for starbursts by Calzetti et al. (1999). The attenuation  $A_\lambda$  for the models is defined as the difference in magnitudes of the stellar luminosity  $L_\lambda$  of a galaxy with and without dust, and is normalized to the colour excess  $E(B - V) = A_B - A_V$  of the stars to give an attenuation “law”  $k(\lambda) = A_\lambda / E(B - V)$ , equiv-

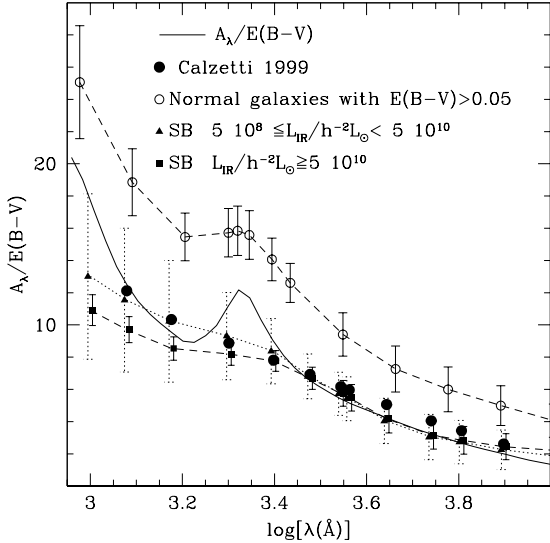


Fig. 11.— The average dust attenuation curves for starlight in different classes of galaxies (normal and starburst, SB) in the model compared with the average Milky Way extinction law (solid line) and with the Calzetti “attenuation law” (filled circles, Calzetti et al. (1999), with  $R_V = 4.05$ ). The attenuation curves are all normalized to the net reddening of the stellar population,  $E(B - V)$ . The error bars show the dispersion of the models around the mean attenuation curve.

alent to the definition of Calzetti et al. . As described in §3.2, the dust properties we adopt imply an extinction law characterized by a distinct 2175 Å feature produced by graphite grains, and well matching the average Milky Way extinction curve. The model extinction law (solid line in Fig. 11) is the attenuation law that would be measured if all the dust were in a foreground screen in front of the stars and no scattered light reached the observer. This geometry is clearly not realistic as applied to the integrated light from galaxies. In our models, we have instead a complex and wavelength dependent geometry, where the UV emitting stars are heavily embedded inside molecular clouds, while the older stars, mainly emitting in the optical and near infrared, are well mixed with the diffuse interstellar medium.

Figure 11 shows average attenuation curves for 3 classes of model galaxies: (a) normal galaxies with  $E(B - V) > 0.05$ ; (b) starbursts with

$5 \times 10^8 < L_{IR} < 5 \times 10^{10} h^{-2} L_{\odot}$ ; and (c) starbursts with  $L_{IR} > 5 \times 10^{10} h^{-2} L_{\odot}$ . The starburst models are all chosen to have ages  $< 50$  Myr since the start of the burst, as discussed in §6.2. Sample (b) corresponds roughly to the galaxies for which Calzetti et al. measured their attenuation law. The model attenuation law depends significantly on the sample, but all 3 classes show a weak or completely absent 2175 Å feature. In particular, the predicted attenuation curve for the lower luminosity starbursts is remarkably close to the empirical “Calzetti law”. This result is an entirely geometrical effect, and did not require us to assume for starbursts dust properties different from those of the Galaxy. This conclusion is contrary to that of Gordon et al. (1997), who argued that the observed shape is only produced with dust that lacks the 2175 Å feature in its extinction curve. The reason is presumably that Gordon et al. only considered clumping of dust, not of stars, and assumed a spatial distribution for stars independent of stellar age. Our results follow naturally from the assumption that stars are born inside dense dust clouds and gradually escape.

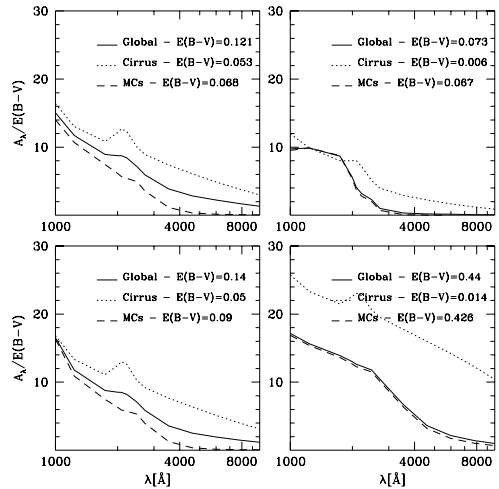


Fig. 12.— Predicted attenuation curves for two normal galaxies (left panels) and two starbursts (right panels) from the models.

To further illustrate the importance of geometrical effects in determining the attenuation law,

we show in Fig. 12 the attenuation laws of 2 normal and 2 starburst model galaxies. The global attenuation law, and the separate contributions from the molecular clouds and diffuse dust, are shown in each case, normalized to the colour excess  $E(B - V)$  produced by that dust component. The global ( $g$ ), molecular cloud (MC) and diffuse dust ( $d$ ) contributions are related by

$$(A_\lambda/E)_g = \frac{(A_\lambda/E)_{MC}E_{MC} + (A_\lambda/E)_dE_d}{E_g} \quad (17)$$

In the far-UV, including the spectral region around the  $2175\text{\AA}$  feature, the global attenuation in the models is strongly contributed, or even dominated, by the MCs. The shape of the attenuation curve there has little to do with the optical properties of grains, because our MCs usually have such large optical depths that the UV light from stars inside the clouds is completely absorbed. The wavelength dependence of the attenuation law of the MC component instead arises from the fact that the fraction of the light produced by very young stars increases with decreasing wavelength, and at the same time, the fraction of stars which are inside clouds increases with decreasing age, as given by eqn. (11). The additional attenuation arising in the cirrus component can sometimes imprint a weak  $2175\text{\AA}$  feature, but this is not the case for the starbursts, where the primary UV stellar light is dominated by very young populations.

## 7. Galaxy Luminosity Function

### 7.1. Method

The luminosity function of galaxies at different wavelengths is a basic property of the galaxy population which a galaxy formation model should explain. We calculate the galaxy luminosity function at different wavelengths by combining the model SEDs with the weights for the individual galaxies (Section 4). For the normal galaxy sample we have, for the number density of galaxies per  $\ln L$  at some wavelength  $\lambda$

$$\frac{dn}{d \ln L_\lambda} = \frac{1}{\Delta \ln L} \sum_{|\ln L_i - \ln L| < \frac{1}{2} \Delta(\ln L)} n_i \quad (18)$$

where  $n_i$  is the number density for the  $i$ th galaxy,  $L_i$  is its luminosity at wavelength  $\lambda$ , the centre of the bin is at  $L$  and its width is  $\Delta(\ln L)$ . For

the burst galaxy sample, we have to sum over the burst phase  $j$  also, giving

$$\frac{dn}{d \ln L_\lambda} = \frac{1}{\Delta \ln L} \sum_{|\ln L_{ij} - \ln L| < \frac{1}{2} \Delta(\ln L)} n_{ij} \quad (19)$$

where  $n_{ij}$  is the number density for galaxy  $i$  at evolutionary phase  $j$ , and  $L_{ij}$  its the luminosity at that phase.

Galaxy luminosity functions are measured in specific bands defined by a filter+instrument response function, e.g. the standard B or K bands, or the IRAS bands. Thus we convolve the model SEDs with the appropriate response function to calculate the luminosity  $L_\nu$  in that band. We use absolute magnitudes on the AB system,  $M_{AB} = -2.5 \log_{10}(L_\nu/4.345 \times 10^{20} \text{erg s}^{-1} \text{Hz}^{-1})$ . The model luminosity functions have statistical uncertainties due to the finite size of the model galaxy catalogue. We estimate these statistical errors by bootstrap resampling of the catalogue.

### 7.2. Optical and Near Infra-Red

At optical and near-IR wavelengths the emission is mostly from older stars and the effects of dust obscuration are generally modest. Figure 13 shows the local luminosity function in the B-band ( $\lambda = 0.44\mu\text{m}$ ), compared to the observed luminosity function measured from the ESP redshift survey by Zucca et al. (1997). The predicted luminosity function agrees well with the observed one, except at the highest luminosities. Extinction by dust makes galaxies around 0.6mag fainter on average, for bright ( $L \gtrsim L_\star$ ) galaxies. Galaxies which have had recent bursts (i.e. in the last 1/20 of the age of the universe, 0.7 Gyr) do not dominate the luminosity function at any luminosity, when the effects of dust are included.

As described in Cole et al. (2000), the B-band luminosity function is used as one of the primary observational constraints for setting the parameters in the GALFORM model, in particular, the parameters  $\alpha_{\text{hot}}$  and  $V_{\text{hot}}$  controlling feedback, and the parameter  $\Upsilon$  which sets the fraction of brown dwarfs in the IMF. The good agreement with the observed B-band luminosity function is therefore not a surprise, but it was not guaranteed, since the stellar population and dust models used in Cole et al. (2000) are not identical to those used here. Cole et al. used the stellar

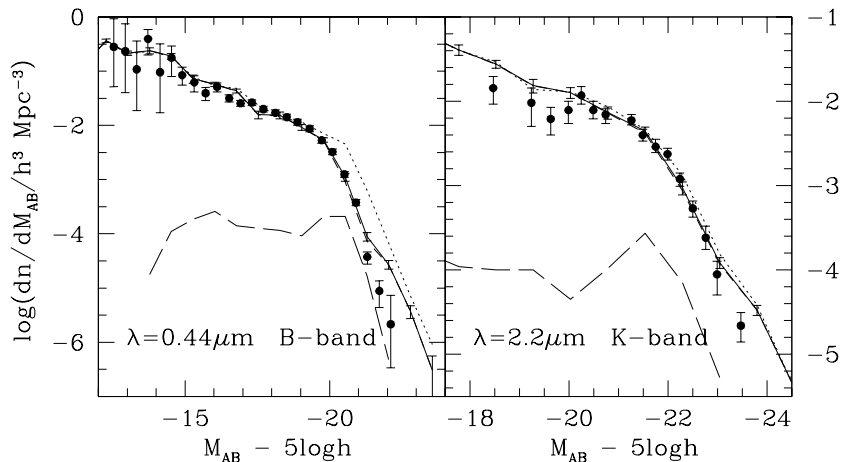


Fig. 13.— Galaxy luminosity functions in the optical and near-IR. The left panel shows the luminosity function in the B-band ( $0.44\mu\text{m}$ ), compared to observational data from Zucca et al. (1997). The right panel shows the luminosity function in the K-band ( $2.2\mu\text{m}$ ), compared to observational data from Gardner et al. (1997). In both panels, the solid line shows the total luminosity function including the effects of dust, while the long-dashed and short-dashed lines show the contributions to this from galaxies with and without recent bursts, and the dotted line shows the luminosity function without dust. The error bars on the model luminosity functions are the statistical errors resulting from the finite sample size, calculated using bootstrap resampling. The observational data have been converted to AB magnitudes assuming  $B = B_J + 0.2$  (to convert from measured to standard magnitudes) and  $B_{AB} = B - 0.12$ , and  $K_{AB} = K + 1.87$  respectively.

population models of Bruzual & Charlot (2000), and calculated the effects of dust using the models of Ferrara et al. (1999). The stellar population model in GRASIL is based on similar stellar evolution tracks and spectra, but the treatment of dust extinction is significantly different. The Ferrara et al. models assume that stars and dust are smoothly distributed, while in GRASIL a fraction of the dust is in clouds, and young stars are confined to these clouds. The B-band luminosity functions, both with and without dust, calculated by GALFORM using the Bruzual & Charlot (2000) and Ferrara et al. (1999) models agree very well with those computed using the GRASIL stellar population+dust model, demonstrating the consistency of the procedure of using the galaxy formation parameters derived in Cole et al. in combination with the GRASIL model. The effects of dust computed using the two models are quite similar in the B-band, in spite of the differences in the star and dust geometry. This is because most of the B-band light is produced by stars which are old enough to have escaped from the clouds in which

they formed, so in GRASIL the attenuation is due mostly to the diffuse component of the dust, which is modelled in a similar way to that in the Ferrara et al. models.

Figure 13 also shows the model and observed luminosity functions in the K-band. In this case, the effects of dust are very small, so the comparison is essentially independent of assumptions about dust. Again, the model agrees well with observations over most of the luminosity range, as was also found by Cole et al. (2000). The contribution of galaxies with recent bursts is very small at all luminosities.

### 7.3. Far Ultra-Violet

In Figure 14 we compare the predicted luminosity function in the far-UV ( $\lambda = 0.2\mu\text{m}$ ) with that measured by Sullivan et al. (2000) from a UV-selected redshift survey, based on FOCA instrument fluxes. This comparison has not previously been made for any semi-analytical galaxy formation models. The effect of dust are much

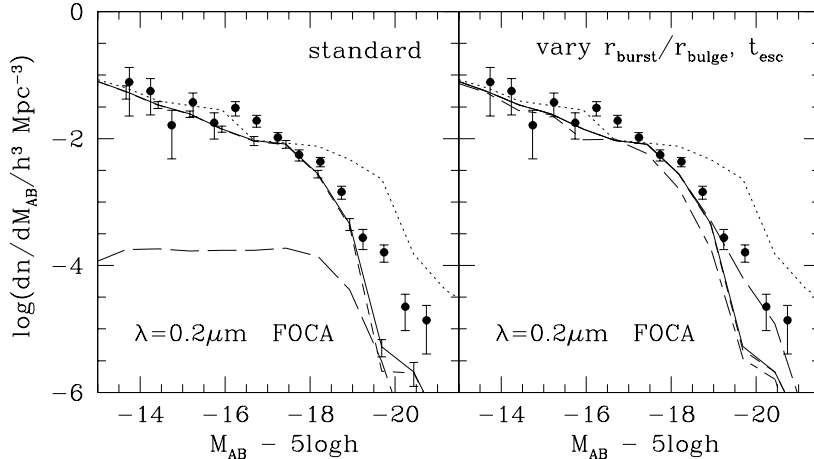


Fig. 14.— Far-UV ( $0.2\mu\text{m}$ ) luminosity function. (a) The left panel shows the results for our standard parameters. The solid line shows the model prediction for the LF at  $z = 0$  including dust, while the long-dashed and short-dashed lines show the contributions to this from galaxies with and without recent bursts. The dotted line shows the model luminosity function obtained if absorption by dust is neglected. The symbols with error bars show the observed  $0.2\mu\text{m}$  luminosity function (without any dust correction) measured from a UV-selected redshift survey by Sullivan et al. (2000). FOCA magnitudes are converted to the AB system, assuming  $m_{AB} = m_{2000} + 2.26$ . (b) The right panel shows the effects of varying  $t_{\text{esc}}$  and  $r_{\text{burst}}$ . The solid line is for our standard model ( $t_{\text{esc}} = 2$  and  $10\text{Myr}$  in normal galaxies and bursts respectively, and  $r_{\text{burst}}/r_{\text{bulge}} = 0.1$ ), including dust. The short-dashed line shows the effect of increasing  $t_{\text{esc}}(\text{burst})$  to  $30\text{Myr}$ , and the short-dash-long-dash line the effect of increasing  $t_{\text{esc}}(\text{normal})$  to  $5\text{Myr}$ . The long-dashed line shows the effect of increasing  $r_{\text{burst}}/r_{\text{bulge}}$  to  $0.5$ . The dotted line shows the LF without dust, which is the same in each of these cases. The observational data are as in the left panel.

larger than in the optical, as one would expect. In this case, the effects of the more realistic geometry for the stars and dust assumed by GRASIL compared to the Ferrara et al. models (clumpy rather than smooth distributions for the stars and dust) are significant. The stars that produce most of the UV light spend a large fraction of their lifetimes in the molecular clouds where they form, so the mean extinction is larger than in the case of a smoothly distributed dust component with the same total dust mass. Bursting and non-bursting galaxies contribute roughly equally at the highest luminosities. This result is however sensitive to the details of how bursts are modelled, since this determines what small fraction of the UV light escapes from currently or recently bursting galaxies. When we compare our model LF including extinction with the directly observed LF, uncorrected for extinction, we find reasonable agreement at lower luminosities, but at high luminosities, the model

LF is somewhat lower than the observed one. This might be partly an effect of evolution in the observational sample, which covers a significant redshift range ( $z \lesssim 0.5$ ), but it might also be that the UV extinction is over-estimated in the model.

Figure 14 shows also the effect of changing the burst radius  $r_{\text{burst}}$  and the timescale  $t_{\text{esc}}$  for stars to escape from clouds. Increasing  $r_{\text{burst}}/r_{\text{bulge}}$  from  $0.1$  to  $0.5$  reduces the optical depth in the diffuse component during bursts, allowing more of the UV light from bursts to escape, and increasing the LF at the highest luminosities. Increasing  $t_{\text{esc}}$  in bursts from  $10\text{Myr}$  to  $30\text{Myr}$  has negligible effect on the total UV LF. Increasing  $t_{\text{esc}}$  in normal galaxies from  $2\text{Myr}$  to  $5\text{Myr}$  slightly lowers the amplitude of the luminosity function at the bright end.



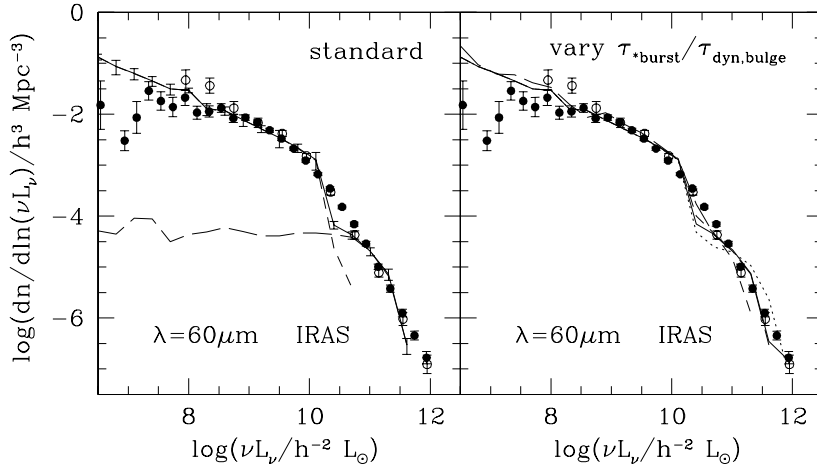


Fig. 15.— The  $60\mu\text{m}$  far-IR luminosity function. (a) The left panel shows the results for our standard parameters. The solid line shows the total model luminosity function, while the long-dashed and short-dashed lines show the contributions to this from galaxies with and without recent bursts. The points with error bars show the observed  $60\mu\text{m}$  luminosity functions measured from galaxies observed by IRAS, by Saunders et al. (1990) (filled circles) and Soifer & Neugebauer (1991) (open circles). (b) The right panel shows the effects of varying the burst or escape timescales:  $\epsilon_{\star\text{burst}}^{-1} \equiv \tau_{\star\text{burst}}/\tau_{\text{bulge}} = 1$  (dotted), 2 (solid), 4 (dashed). The long dashed curve has  $\epsilon_{\star\text{burst}}^{-1} = 2$  (our standard value) but  $t_{\text{esc}} = 2$  Myr instead of 5 Myr.

#### 7.4. Mid and Far Infra-Red

In the mid- and far-infrared, the luminosity of galaxies is dominated by re-emission from dust. Using the GRASIL code, we can now directly predict the far-IR luminosities of galaxies from our galaxy formation model, and compare with observations. The luminosity functions of galaxies at 12, 25, 60 and  $100\mu\text{m}$  have been measured using IRAS data. The best determination is at  $60\mu\text{m}$ , where IRAS was most sensitive. Figure 15 shows that the predicted luminosity function agrees extremely well with that observed by Saunders et al. (1990) and Soifer & Neugebauer (1991), except at very low luminosities, where the measured LF is fairly uncertain. Above  $\nu L_{\nu}(60) \gtrsim 3 \times 10^{10} h^{-2} L_{\odot}$ , the model LF is dominated by galaxies undergoing bursts triggered by mergers. This is in agreement with observations of ultra-luminous IRAS galaxies, which are all identified as recent mergers based on their optical morphology (e.g. Sanders & Mirabel 1996).

The right panel of Figure 15 shows the effect on the  $60\mu\text{m}$  LF of varying the parameter  $\epsilon_{\star\text{burst}}$ , which relates the star formation timescale

in bursts to the dynamical time of the bulge (equation 6). Unlike the other parameters in the GALFORM model, Cole et al. (2000) did not try to choose a best-fit value, because the observational data in the optical and near-IR that they compared with were not sensitive to its value. (The Cole et al. results were calculated assuming  $\tau_{\star\text{burst}} = 0$ .) However, the far-IR LF is sensitive to this and thus constrains the burst timescale for the most luminous galaxies. Figure 15 shows predictions for  $\epsilon_{\star\text{burst}} = 1, 0.5, 0.25$ , corresponding to  $\tau_{\star\text{burst}}/\tau_{\text{bulge}} = 1, 2, 4$  respectively. Increasing  $\epsilon_{\star\text{burst}}$  means bursts are more luminous, but last for a shorter time, and so have a lower number density. This trend is seen at the high-luminosity end of the  $60\mu\text{m}$  LF, which is dominated by bursting galaxies. A value  $\epsilon_{\star\text{burst}} = 2$  seems to fit somewhat better than higher or lower values, so we adopt this as our standard value. Also shown in the same panel is the somewhat better fit obtained setting  $t_{\text{esc}} = 5$  Myr. However, as explained in § 3.3, our adopted standard value 2 Myr is favored by stellar evolution timescale argument and by the UV LF. Increasing  $t_{\text{esc}}$  in bursts from 10 Myr to

30Myr has negligible effect on the LF.

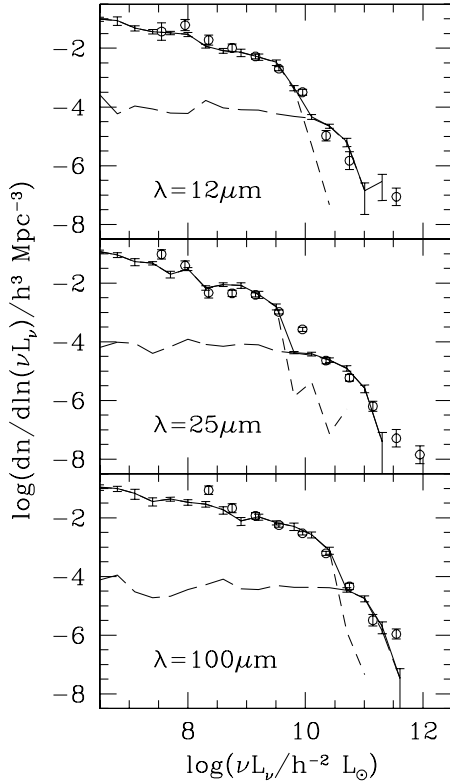


Fig. 16.— The luminosity functions in the 12, 25 and  $100\mu\text{m}$  IRAS bands, compared to observational data from Soifer & Neugebauer (1991). The line types and symbols are as in Fig.15.

The luminosity functions at 12, 25 and  $100\mu\text{m}$ , are compared with the observational data from Soifer & Neugebauer (1991) in Figure 16. The predicted luminosity function agrees well with the measured one in each case.

### 8. Star formation rate indicators

Here we examine the accuracy of several SFR indicators based on continuum UV or IR luminosities (reviewed by e.g. Kennicutt 1999).

The luminosity  $L_\nu(2800)$  at  $2800\text{\AA}$  has been extensively used to estimate SFRs of high-redshift galaxies and to investigate the evolution of the cosmic SFR density (e.g. Lilly et al. 1996; Conolly et al. 1997). In the top panel of Fig. 17, we plot the SFR against  $L_\nu(2800)$  for the model galaxies,

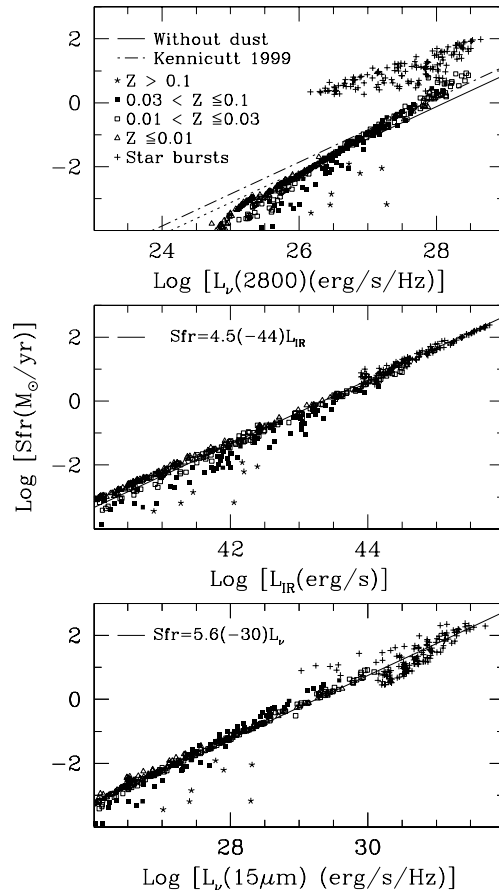


Fig. 17.— Star formation rate versus UV and IR luminosities for galaxies from our model. Only models corresponding to spirals and luminous starburst galaxies are plotted. See text for details.

including the effects of extinction. Only models corresponding to spiral galaxies ( $B/T \leq 0.5$ ) and luminous starburst galaxies ( $L_{IR} \geq 10^{10} h^{-2} L_\odot$ ) are shown. At higher luminosities and SFRs,  $L_\nu(2800) \gtrsim 3 \times 10^{26} \text{erg s}^{-1} \text{Hz}^{-1}$ , the models *in the absence of dust* follow a linear relation between SFR and  $L_\nu$ , with a rather small dispersion, as would be expected if the UV luminosity is dominated by young stars and the recent SFR has been approximately constant. This linear relation,  $SFR/(M_\odot \text{yr}^{-1}) = 8.5 \times 10^{-29} L_\nu(2800\text{\AA})/(\text{erg s}^{-1} \text{Hz}^{-1})$ , is indicated by the solid line, and its extrapolation to lower luminosity is shown by the dotted line. Dust extinction

shifts points to the left of this line. At lower luminosities, the effects of dust extinction are very small, because of the low gas contents of the galaxies. On the other hand, because the SFRs are so small, the  $2800\text{\AA}$  light has a significant contribution from post-AGB stars and old metal poor populations, and this causes the locus of points to bend to the right of the linear relation. The galaxies with very high metallicities ( $Z > 0.1$ ) have very low gas fractions.

The figure also shows as a dashed line the linear relation between  $L_\nu(2800)$  and SFR obtained by Kennicutt (1999), using stellar population models for a Salpeter IMF, and assuming a constant SFR for the last  $10^8\text{yr}$ . The  $SFR/L_\nu$  ratio in our models without dust (solid line) is about 40% lower than Kennicutt's value, but this difference is entirely due to the different IMF we adopt (equation (9)).

Perhaps the most striking feature of this plot is that the starburst models are offset by more than an order of magnitude from the average relation holding for the normal spirals, because of the large UV extinctions in the starbursts. Furthermore, their dispersion in SFR at a given luminosity is also quite large. Thus, the  $2800\text{\AA}$  luminosity with no dust correction performs rather poorly as a quantitative SFR indicator, both for very high SFRs (because of extinction) and for very low ones (because of the light from older stars).

The middle panel of Fig.17 depicts the relation between the star formation rate and  $L_{IR}$  (eq. 16), the estimated  $8 - 1000\mu\text{m}$  luminosity based on the IRAS fluxes. The solid line represents the relation derived by Kennicutt (1998) for starbursts,  $SFR/(M_\odot\text{yr}^{-1}) = 4.5 \times 10^{-44} L_{IR}/(\text{erg s}^{-1})$ , by assuming that the bolometric output in a continuous burst of age between 10–100 Myr is completely reprocessed by dust, again for a Salpeter IMF. The Kennicutt relation is seen to fit our model galaxies quite well at all luminosities (normal spirals as well as starbursts), even though we assume a different IMF from Kennicutt.

The luminosity in the ISO  $15\mu\text{m}$  band has also been proposed as an approximate SFR indicator. The bottom panel of Fig. 17 shows the SFR vs  $L_\nu(15\mu\text{m})$  for our galaxies. The line plotted is our best linear fit to the model points,  $SFR/(M_\odot\text{yr}^{-1}) = 5.6 \times 10^{-30} L_\nu(15\mu\text{m})/(\text{erg s}^{-1}\text{Hz}^{-1})$ . Despite the important contribution from PAH

bands, the correlation of the SFR with  $L_\nu(15\mu\text{m})$  in our models is still fairly good.

## 9. Summary and Conclusions

We have combined an *ab initio* model of galaxy formation (GALFORM, §2, Cole et al. 2000), with an *ab initio* model for stellar emission and dust emission and absorption in galaxies (GRASIL, §3, Silva et al. 1998). Both models are state-of-the-art. We are able to predict, in the context of the cold dark matter cosmology, the luminosities and spectral energy distributions from the UV to the sub-mm for the whole galaxy population, and how these change with cosmic epoch. Here we focused on a wide range of spectrophotometric properties of present-day galaxies, from the UV to the sub-mm, for a flat low-density cosmology ( $\Omega_0 = 0.3$ ,  $\Lambda_0 = 0.7$ ) with a CDM spectrum of density fluctuations. The model is remarkably successful in explaining the UV, optical and IR spectrophotometric and extinction properties of galaxies in the local universe. Future papers will investigate galaxy evolution in the UV, optical, IR and sub-mm out to high redshift.

Dust plays a dominant role in starburst galaxies, where star formation proceeds in the central regions of a galaxy on a short timescale. We did not previously make any detailed comparison of the properties of the starbursts predicted by semi-analytical galaxy formation models with observational data. Here we have shown that these properties are nicely reproduced.

Our model predicts an average dust attenuation law for starburst galaxies that agrees remarkably well with the empirical law found by Calzetti et al. (1999), although with a significant dispersion around the mean. In particular, the  $2175\text{\AA}$  bump is absent when the net attenuation of the galaxy light is considered. This is entirely an effect of the geometry of stars and dust in our model, and has nothing to do with the optical properties of dust grains. Indeed, our dust mixture would reproduce the average Milky Way extinction curve (with a strong  $2175\text{\AA}$  feature), if it were arranged in a foreground screen geometry. The absence of this feature in the attenuation curves of model starbursts is because in that case the dust attenuation is dominated by molecular clouds, with the shape controlled by the gradual escape of young

stars from the clouds.

The starburst galaxies are predicted to dominate the bright end of the luminosity function in terms of bolometric luminosity, but because of the large extinctions in these objects, they do not make a dominant contribution to the bright end of the luminosity function in either the UV, optical or near-IR once dust effects are included. At these wavelengths, the luminosity function is dominated by normal spiral and elliptical galaxies. However, the starbursts completely dominate the bright end of the luminosity function in the mid- and far-IR (10–100 $\mu$ m), at total luminosities  $L_{IR} \gtrsim 10^{11} h^{-2} L_{\odot}$ . Overall, the luminosity function predictions from the far-UV to the far-IR are a remarkable success for the model, since the dust contents and galaxy radii are predicted *a priori*, and the only significant adjustable parameter in the comparison was the ratio of the burst timescale to the bulge dynamical time, which was chosen to fit the bright end of the luminosity function at 60 $\mu$ m.

As expected, our models show that the UV continuum is in general a poor star formation indicator, both because of the large variations in the amount of extinction, and also because of the contribution from old stellar populations in the mid-UV ( $\sim 3000\text{\AA}$ ) in more quiescent galaxies. The infrared luminosity is a much more reliable SFR indicator.

The parameters values adopted here for the GALFORM model are those chosen previously by Cole et al. (2000) to fit the properties of the local galaxy population in the optical and near-infrared, apart the new ones specifying the timescales and radii of bursts. Cole et al. also discuss the effects of varying the 'old' GALFORM parameters. The purpose of this paper was to present the effects of including dust in a fixed galaxy formation model. The treatment of dust reprocessing with GRASIL requires some additional parameters to be set, but opens the possibility to test semi-analytical models against the wealth of IR and sub-mm observations already available or planned for the near future. The adopted values for these parameters have also been guided by the results of Silva et al. (1998), who used GRASIL to reproduce detailed SEDs of several local normal and starburst galaxies. Some of the effects of variations of these parameters on SEDs, LFs and starburst properties

have been discussed in the relevant sections of this paper. A more systematic parameter study will be included in future investigations. Among the newly introduced parameters, probably the most important ones are  $\epsilon_{\star\text{burst}}$  and  $t_{\text{esc}}$ , describing the timescales of bursts and the time for young stars to escape from their parent molecular clouds. They have significant effects on (and are constrained by) the IR and UV luminosity functions respectively.

In conclusion, this paper is a stepping stone for future work, which will apply the same models to galaxies at high redshift. Now that semi-analytic models can be effectively compared with infrared and sub-millimetre observations, as well as UV and optical data, they can be used to work towards an observationally and theoretically consistent picture for the history of galaxy formation and star formation in the universe.

We thank the anonymous referee for a constructive report. We acknowledge the support by the European Community under TMR grant ERBFMRX-CT96-0086. SMC acknowledges the support of a PPARC Advanced Fellowship, and CSF a PPARC Senior Fellowship and a Leverhulme Research Fellowship. CGL acknowledges the support of the Danish National Research Foundation through its establishment of the TAC, and a PPARC Visiting Fellowship at Durham. This work was partially supported by the PPARC rolling grant for extragalactic astronomy and cosmology at Durham.

## REFERENCES

- Almaini, O., Lawrence, A., Boyle, B.J., 1999, MNRAS, 305, L59
- Alton, P. B., et al. 1998, A&A, 335, 807
- Armus, L, Heckman, T., Miley, G, 1990, ApJ, 364, 471
- Balzano, V.A., 1983, ApJ, 268, 602
- Baugh, C.M., Cole, S., Frenk, C.S., 1996b, MNRAS, 283, 1361
- Baugh, C. M., Cole, S., Frenk, C. S., Lacey, C.G., 1998, ApJ, 498, 504
- Baugh, C.M., Benson, A.J., Cole, S., Frenk, C.S., Lacey, C.G., 1999, MNRAS, 305, L21

- Benson, A.J., Cole, S., Frenk, C.S., Baugh, C.M., Lacey, C.G., 2000, MNRAS, 311, 793
- Boulanger, F., Boissel, P., Cesarsky, D., Ryter, C., 1998, A&A, 339, 194
- Bressan, A., Chiosi, C., Fagotto, F. 1994, ApJS, 94, 63.
- Bressan, A., Granato, G.L., Silva, L. 1998, A&A, 332, 135.
- Bruzual, G., Charlot, S., 2000, *in preparation*
- Buat, V., & Xu, C., 1996, A&A, 306,61
- Calzetti, D., 1994, AJ, 113, 162
- Calzetti, D., 1999, *UV Emission and Dust Properties of High Redshift Galaxies, Workshop on Ultraluminous Galaxies: Monsters or Babies*, Ringberg Castle, Germany, Kluwer, in press (astro-ph/9902107)
- Calzetti, D., Armus, L., Bohlin, R.C., Kinney, A.L., Koornneef, J., Storchi-Bergmann, T., 1999, accepted for publication in ApJ(astro-ph/9911459)
- Calzetti, D., Kinney A., L., Storchi-Bergmann, T., 1994, ApJ, 429, 582
- Cole, S., Aragón-Salamanca, A., Frenk, C.S., Navarro, J.F., Zepf, S.E., 1994, MNRAS, 271,781
- Cole S., Lacey C. G., Baugh C. M., Frenk C. S., 2000, submitted to MNRAS
- Conolly, A.J., Szalay, A.S., Dickinson, M., SubbaRao, M.U., Brunner, R.J., 1997, ApJ, 486, L11
- Diaferio, A., Kauffmann, G., Colberg, J.M., White, S.D.M., 1999, MNRAS, 307, 537.
- Dwek, E., et al. 1998, ApJ, 508, 106
- Elbaz, D., et al. 1999, A&A, 351, L37
- Ferrara, A., Bianchi, S., Cimatti, A., Giovanardi, C., 1999, ApJS, 123, 437
- Fitzpatrick, E. 1989, IAU Symp. 135: Interstellar Dust, 135, 37
- Fixsen, D.J., Dwek, E., Mather, J.C., Bennett, C.L., Shafer, R.A., 1998, ApJ, 508, 123
- Flores, H, et al. 1999, ApJ517, 148
- Franceschini, A., Mazzei, P., de Zotti, G., Danese, L., 1994, ApJ, 427, 140
- Gardner, J.P., Sharples, R.M., Frenk, C.S., Carrasco, B.E., ApJ, 480, L99
- Giovanelli, R., Haynes, M.P., Salzer, J.J., Wegner, G., da Costa, L.N., & Freudling, W., 1995, AJ, 110, 1059
- Gordon, K.D., Calzetti, D., Witt, A.N., 1997, ApJ, 487, 625
- Governato, F., Baugh C. M., Frenk C. S., Cole S., Lacey C. G.,Quinn, T. Stadel, J., 1998, Nature, 392, 359
- Granato, G.L., Danese, L. & Franceschini, A., ApJ, 486, 147
- Guiderdoni, B., Rocca-Volmerange, B., 1987, A&A, 186, 1
- Guiderdoni, B. , Bouchet, F. R., Puget, J. -L. , Lagache, G. & Hivon, E. 1997, Nature, 390, 257
- Guiderdoni, B., Hivon, E., Bouchet, F.R., Maffei, B., 1998, MNRAS, 295, 877
- Hauser, M.G., et al. , 1998, ApJ, 508, 25
- Heckman T. M., Robert C., Leitherer C., Garnett D.R. & ven der Rydt F. 1998, ApJ, 503, 646
- Helou, G., Khan, I.R., Malek, L., Boehmer, L., 1988, ApJS, 68, 151
- Hughes, D.H., et al. , 1998, Nature, 394, 241
- Jenkins, A., Frenk, C.S., Pearce, F.R., Thomas, P.A., Colberg, J.M., White, S.D.M., Couchman, H.M.P., Peacock, J.A., Efstathiou, G., Nelson, A.H., (the VIRGO consortium), 1998, ApJ, 499, 20
- de Jong, R.S., 1996c, A&A, 313, 377
- de Jong, R.S. van der Kruit 1994, A&ASupp 106, 451

- Kauffmann, G., White, S.D.M., Guiderdoni, B., 1993, MNRAS, 264, 201
- Kauffmann, G., 1996, MNRAS, 281, 487
- Kauffmann, G., Nusser, A., Steinmetz, M., 1996, MNRAS, 281, 487
- Kauffmann, G., Colberg, J.M., Diaferio, A., White, S.D.M., 1999, MNRAS, 303, 188
- Kawara, K., et al. 1998, A&A, 336, L9
- Kennicutt, R.C., 1983, ApJ, 272, 54
- Kennicutt, R.C., 1998, ApJ, 498, 541
- Kennicutt, R.C., 1999, ARA&A, 36, 189
- Keto, E., Ball, R., & Arens, J., Jernigan, G., Meixner, M., 1992, ApJ, 387, L17
- Kinney, A.L., Bohlin, R.C., Calzetti, D., Panagia, N., Wyse, R.F.G., 1993, ApJS, 86, 5
- Kylafis, N.D., & Bahcall, J.N., 1987, ApJ, 317, 637
- Lacey, C.G., Granato, G., Silva, L., Bressan, A., Baugh, C., Cole, S., Frenk, C.S., 2000, in preparation
- Lacey, C.G., Guiderdoni, B., Rocca-Volmerange, B., Silk, J., 1993, ApJ, 402, 15
- Lacey, C.G., Silk, J., 1991, ApJ, 381, 14
- Lehnert, M., & Heckman, T., 1995, ApJS, 97, 89
- Lilly, S.J., LeFevre, O., Hammer, F., Crampton, D., ApJ, 460, L1
- Lilly, S.J., Eales, S.A., Gear, W.K., Hammer, F., LeFevre, O., Crampton, D., Bond, J.R., Dunne, L., 1999, ApJ, 518, 641
- Lisenfeld, U., Isaak K., G., Hills, R. 2000, MNRAS, 312, 433
- Madau, P., 1999, in "VLT Opening Symposium" (astro-ph/9907268)
- Madau, P., Ferguson, H.C., Dickinson, M., Giavalisco, M., Steidel, C.C., Fruchter, A., 1996, MNRAS, 283, 1388
- Madau P., Pozzetti L., Dickinson M., 1998, ApJ, 498, 106
- Mazzei, P., Xu, C., de Zotti, G., 1992, A&A, 256, 45
- Meurer, G.R., Heckman, T.M., Leitherer, C., Kinney, A., Robert, C., Garnett, D.R. 1995, AJ 110, 2665
- Oliver, S. J., et al. 1997, MNRAS, 289, 471
- Pearson, C., Rowan-Robinson, M., 1996, MNRAS, 238, 523
- Pettini, M., Kellogg, M., Steidel, C., Dickinson, M., Adelberger, K.L., Giavalisco, M., 1998, ApJ, 508, 539
- Press W. H., Schechter P., 1974, ApJ, 187, 42
- Puget, J.L, et al. 1996, A&A, 308, L5
- Puget, J. L., et al. 1999, A&A, 345, 29
- Sage, L.J., 1993, A&A, 272, 123
- Sanders, D.B., Mirabel, I.F. , 1996, Ann Rev 34, 749
- Scalo, J., 'The Stellar Initial Mass Function', ASP conference series Vol. 142, eds. G. Gilmore & D. Howell, p.201 (ASP: San Francisco)
- Saunders, W., 1997, private communication
- Saunders, W., Rowan-Robinson, M., Lawrence, A., Efstathiou, G, Kaiser, N., Ellis, R.S., Frenk, C.S., 1990, MNRAS, 242, 318
- Schlegel, D.J., Finkbeiner, D.P., Davis, M., 1998, ApJ, 500, 525
- Scoville, N.Z., Yun, M.S., Bryant, P.M., 1997, ApJ, 484, 702
- Silva, L., Granato, G.L., Bressan, A., Danese, L., 1998, ApJ, 509, 103
- Simien, F., de Vaucouleurs, G., 1986, ApJ, 302, 564
- Smail, I., Ivison, R.J., Blain, A.W., 1997, ApJ, 490, L5
- Soifer, B.T., Boehmer, L., Neugebauer, G., Sanders, D.B., 1989, AJ, 98, 766
- Soifer, B.T., Neugebauer, G., 1991, AJ, 101, 354

- Somerville, R.S., Primack, J.R., 1999, MNRAS, 310, 1087
- Steidel, C.C., Adelberger, K.L., Giavalisco, M., Dickinson, M., Pettini, M., 1999, ApJ, 519, 1
- Sullivan, M., Treyer, M.A., Ellis, R.S., Bridges, T.J., Milliard, B., Donas, J., 2000, MNRAS, 312, 412
- Thuan, T.X., Martin, G.E., 1981, ApJ, 247, 823
- Tully, R.B., Pierce, M.J., Huang, J. Saunders, W., Verheijen, M.A.W., Witchalls, P.L., 1998, AJ, 115, 2264
- de Vaucouleurs, G., de Vaucouleurs, A., Corwin, H.G., Buta, R.J., Paturel, G., Fouque, P., 1991, Third Reference Catalogue of Bright Galaxies (New York: Springer)
- Wang, B., & Heckman, T., 1996, ApJ, 457, 645
- White, S.D.M., Frenk, C.S., 1991, ApJ, 379, 25
- Wright, G.S., James, P.A., Joseph, R.D., McLean, I.S., 1990, Nature, 344, 417
- Xilouris, E.M., Byun, Y.I., Kylafis, N.D., Paleologou, E.V., Papamastorakis, J., A&A, 344, 868
- Xu, C., & Buat, V., 1995, A&A, 293, L65
- Wang, B. 1991, ApJ, 374, 465
- Zucca, E., et al. , 1997, A&A, 326, 477